Numer. Math. Theor. Meth. Appl.
doi: 10.4208/nmtma.2014.1218nm

Vol. 7, No. 3, pp. 288-316
August 2014

Evaluating Local Approximations of the L^2-Orthogonal Projection Between Non-Nested Finite Element Spaces

Thomas Dickopf* and Rolf Krause

Università della Svizzera italiana (USI, University of Lugano), Institute of Computational Science, Via G. Buffi 13, 6904 Lugano, Switzerland.

Received 31 July 2012; Accepted (in revised version) 1 March 2014

Available online 12 August 2014

Abstract. We present quantitative studies of transfer operators between finite element spaces associated with unrelated meshes. Several local approximations of the global L^2-orthogonal projection are reviewed and evaluated computationally. The numerical studies in 3D provide the first estimates of the quantitative differences between a range of transfer operators between non-nested finite element spaces. We consider the standard finite element interpolation, Clément's quasi-interpolation with different local polynomial degrees, the global L^2-orthogonal projection, a local L^2-quasi-projection via a discrete inner product, and a pseudo-L^2-projection defined by a Petrov-Galerkin variational equation with a discontinuous test space. Understanding their qualitative and quantitative behaviors in this computational way is interesting per se; it could also be relevant in the context of discretization and solution techniques which make use of different non-nested meshes. It turns out that the pseudo-L^2-projection approximates the actual L^2-orthogonal projection best. The obtained results seem to be largely independent of the underlying computational domain; this is demonstrated by four examples (ball, cylinder, half torus and Stanford Bunny).

AMS subject classifications: 65D05, 65F10, 65N30, 65N50, 65N55

Key words: Finite elements, unstructured meshes, non-nested spaces, transfer operators, interpolation, projection.

1. Introduction

The question of how to interpolate functions in finite element spaces is as old as the finite element method itself. Approximation operators which map a given function to a finite element space appear frequently in numerical analysis for a variety of reasons. For both a priori and a posteriori discretization error estimates, one often needs to

*Corresponding author. *Email addresses:* thomas.dickopf@usi.ch (T. Dickopf), rolf.krause@usi.ch (R. Krause)

treat general elements of infinite dimensional function spaces. However, such operators are usually not evaluated computationally but merely used in the analysis. A famous example is the early work by Clément [26] on finite element quasi-interpolation of discontinuous (non-smooth) functions.

In this paper, we study different operators mapping to finite element spaces. Although a couple of the reviewed properties hold true in case the input function is in an infinite dimensional function space, our main focus is the information transfer between two finite element spaces. We investigate this by a series of numerical studies. The respective spaces are Lagrange conforming finite elements of first order associated with (either two or a whole hierarchy of) non-nested meshes. This non-nested information transfer is important, for instance, in non-conforming domain decomposition methods [8,9,41,62,63] or in domain decomposition or multigrid methods with non-nested coarse spaces [11, 15, 18, 20, 24, 30, 47, 48, 65] for the solution of partial differential equations. It appears both in the analysis and in practical computations.

We present computational results on the behavior of local approximations of the L^2-projection between non-nested finite element spaces. Our numerical studies are based on a detailed overview of different transfer operators. Let us emphasize that there is neither a conclusive characterization of the information transfer between finite element spaces associated with non-nested meshes nor a comprehensive classification of transfer operators in this setting yet. In the present investigations, we show that, apart from basic similarities, there are substantial conceptual and qualitative differences as well as substantial quantitative differences between the studied operators.

Our research is in part motivated by the fundamental work on quasi-interpolation [26, 54]. We also learned about advanced techniques for the construction of transfer operators from [41, 62, 63] in the context of non-conforming domain decomposition methods. Other interesting studies giving basic insights into the analysis of approximation operators in finite element spaces, which influenced our work, can be found in [4, 12, 13, 20, 24, 56–58, 64].

The evaluation criteria that are discussed in the theoretical part are the H^1-stability, an L^2-approximation property, the locality of the information transfer, and the projection properties. In the computational part, we study the mutual relations between the diverse transfer operators by numerical experiments. The operators are evaluated for four examples of computational domains (ball, cylinder, half torus and Stanford Bunny), each time for a series of independently generated meshes. All distances with respect to certain operator norms are computed by solving the corresponding generalized eigenvalue problems. To our knowledge, similar studies estimating distances between transfer operators in the present context cannot be found elsewhere.

Let us briefly comment on an application for the non-nested information transfer studied in this paper to multilevel preconditioners, which are among the most efficient algorithms for the solution of discretized partial differential equations in many applications; see, e.g., [5, 14, 17, 39, 40, 46, 50, 59, 66] for some of the most influential achievements. For applications in computational engineering involving complicated geometries in three dimensions, the construction of coarse spaces is often demanding

and a flexible choice requires suitable transfer operators. In case of elliptic problems discretized with first order elements on unstructured meshes, it is known from the literature on domain decomposition methods [20, 24, 30, 58, 65] that coarse spaces associated with non-nested meshes can be applied successfully to construct efficient preconditioners. This holds true both for two-level overlapping Schwarz methods with global coarse space and for multigrid methods. These classes of methods can be constructed either in a variational or in a non-variational setting. The first one is characterized by a recursive Galerkin relation whereas the second one works with virtually independent coarse level problems. In any case, transfer operators between finite element spaces associated with non-nested meshes are necessary ingredients.

Outline This paper is organized as follows. In the remainder of Section 1, we introduce useful notations concerning the information transfer in finite element spaces and comment on characteristic properties of transfer operators. Section 2 is the first main part where different transfer operators are investigated comprehensively. Here, we also comment on a uniform H^1-stability estimate for the one-dimensional nodal interpolation. In a second main part, Section 3, we present the quantitative studies of the diverse transfer operators and their mutual relations for three geometric shapes in 3D. Section 4, is devoted to numerical studies for a more complex geometry (Stanford Bunny).

1.1. Operators between finite element spaces associated with non-nested meshes

We recall several standard notations from functional analysis; see, e.g., [1,35]. The Lebesgue integral is denoted by $\int \cdot \, d\boldsymbol{x}$. For a Lipschitz domain $\Omega \subset \mathbb{R}^d$, let $L^2(\Omega)$ be the Hilbert space of square integrable functions in Ω with inner product $(v,w)_{L^2(\Omega)} := \int_\Omega vw \, d\boldsymbol{x}$ and norm $\|\cdot\|_{L^2(\Omega)} := (\cdot,\cdot)_{L^2(\Omega)}^{1/2}$. The symbol $L^\infty(\Omega)$ represents the space of essentially bounded functions with norm $\|v\|_{L^\infty(\Omega)} := \operatorname{ess\,sup}_{\boldsymbol{x}\in\Omega} |v(\boldsymbol{x})|$. By $H^m(\Omega)$, as customary, we denote the Sobolev space of functions with $m \geq 1$ square integrable weak derivatives in Ω. Let $\alpha \in \mathbb{N}^d$ be a multi-index of order $|\alpha| := \sum_{1\leq i\leq d} \alpha_i$. Then, ∂^α denotes the weak differentiation and the corresponding norm and semi-norm in $H^m(\Omega)$ are

$$\|v\|_{H^m(\Omega)} := \left(\sum\nolimits_{|\alpha|\leq m} \|\partial^\alpha v\|_{L^2(\Omega)}^2\right)^{1/2} \quad \text{and} \quad |v|_{H^m(\Omega)} := \left(\sum\nolimits_{|\alpha|=m} \|\partial^\alpha v\|_{L^2(\Omega)}^2\right)^{1/2}.$$

Moreover, the subspace of $H^1(\Omega)$ with vanishing image of the usual trace operator to the boundary $\partial\Omega$ is called $H_0^1(\Omega)$; we have $H_0^1(\Omega) = \{v \in H^1(\Omega) \mid v|_{\partial\Omega} = 0 \text{ in } H^{1/2}(\partial\Omega)\} = \{v \in H^1(\Omega) \mid v = 0 \text{ a.e. on } \partial\Omega\}$.

Let $(\mathcal{T}_\ell)_{\ell\in\mathbb{N}}$ be a family of *non-nested* shape regular meshes (i.e., of non-overlapping decompositions into finitely many open polytopes) of Lipschitz domains $(\Omega_\ell \subset \mathbb{R}^d)_{\ell\in\mathbb{N}}$ of dimension $d \in \{2,3\}$, i.e., there is a constant c such that $\sup_{\ell\in\mathbb{N}} \max_{T\in\mathcal{T}_\ell} h_T/r_T \leq c$.

Here, for an element $T \in \mathcal{T}_\ell$, let $h_T := \operatorname{diam}(T)$ be the diameter of T and r_T the radius of the largest ball inscribed in T. For simplicity, assume $\Omega_\ell \subset \Omega_{\ell-1}$ for $\ell > 0$. We say $(\mathcal{T}_\ell)_{\ell\in\mathbb{N}}$ is quasi-uniform if, in addition, there is another constant c, independent of ℓ, such that $\max_{T\in\mathcal{T}_\ell} h_T \le c \min_{T\in\mathcal{T}_\ell} h_T$ for all $\ell \in \mathbb{N}$. As usual, local mesh size functions $h_\ell \in L^\infty_>(\Omega_\ell) := \{v \in L^\infty(\Omega_\ell) \mid \exists\ \alpha > 0,$ such that $v(\boldsymbol{x}) > \alpha$ for a.e. $\boldsymbol{x} \in \Omega_\ell\}$ are introduced for instance defined a.e. by $h_\ell(\boldsymbol{x}) := h_T$ if $\boldsymbol{x} \in T$. Assume the sequence $(h_\ell)_{\ell\in\mathbb{N}}$ is decreasing where well-defined.

We denote the set of nodes of $\mathcal{T}_\ell$ by $\mathcal{N}_\ell$ and abbreviate $n_\ell := |\mathcal{N}_\ell|$. At each level ℓ, we consider the space X_ℓ of Lagrange conforming finite elements of first order and denote its nodal basis as $\Lambda_\ell = (\lambda_p^\ell)_{p\in\mathcal{N}_\ell}$ with $\lambda_p^\ell(q) = \delta_{pq}$, $p, q \in \mathcal{N}_\ell$. Let $\omega_p := \operatorname{supp}(\lambda_p^\ell)$ be the support of the basis function at node $p \in \mathcal{N}_\ell$ commonly called patch. We occasionally use coordinate isomorphisms of the form $\Phi_\ell : \mathbb{R}^{n_\ell} \to X_\ell$, $\Phi_\ell(\boldsymbol{v}) := \sum_{p\in\mathcal{N}_\ell} v_p \lambda_p^\ell$. See [25].

This paper is devoted to the numerics of the information transfer between non-nested finite element spaces. A generic or unspecific transfer operator is denoted by Π. To every concrete operator we will assign a different calligraphic symbol ($\mathcal{I}$, $\mathcal{P}$, $\mathcal{Q}$, $\mathcal{R}$), sometimes varied by a tilde. If an operator maps between the two (non-nested) spaces $X_{\ell-1}$ and X_ℓ, this will be indicated by, e.g., $\Pi_{\ell-1}^\ell$. Similarly, an operator mapping some other space, such as a Lebesgue or Sobolev space, to the finite element space X_ℓ will be denoted by, e.g., Π_ℓ. This shall suggest that a mesh $\mathcal{T}_\ell$ with a local mesh size function $h_\ell \in L^\infty_>(\Omega_\ell)$ is always involved. A matrix $\boldsymbol{\Pi}_{\ell-1}^\ell \in \mathbb{R}^{n_\ell \times n_{\ell-1}}$ represents an operator $\Pi_{\ell-1}^\ell$ with respect to the chosen bases if $\Pi_{\ell-1}^\ell v = \Phi_\ell(\boldsymbol{\Pi}_{\ell-1}^\ell \Phi_{\ell-1}^{-1}(v))$ for all $v \in X_{\ell-1}$.

1.2. On the properties of transfer operators

In this section, we briefly review characteristic properties of transfer operators which are studied in this paper. Naturally, one does not only examine single entities but rather considers entire types or families of transfer operators. For example, the terms "linear interpolation" or "orthogonal projection" specify different instructions each providing an operator $\Pi : X \to Y$ depending on certain data, namely the domains $\Omega_Y \subset \Omega_X \subset \mathbb{R}^d$ and the spaces $X \subset H^1(\Omega_X)$ and $Y \subset H^1(\Omega_Y)$. In this paper, the target space Y is always a finite element space.

Definition 1.1. *Let $\Omega_Y \subset \Omega_X \subset \mathbb{R}^d$ be domains. Given a subspace $X \subset H^1(\Omega_X)$ and a (target) finite element space $Y \subset H^1(\Omega_Y)$ with discretization parameter $h_Y \in L^\infty_>(\Omega_Y)$, an operator $\Pi : X \to Y$ is called H^1-stable in X if*

$$|\Pi v|_{H^1(\Omega_Y)} \lesssim |v|_{H^1(\Omega_X)}, \quad \forall\, v \in X. \tag{1.1}$$

We say that the operator Π satisfies the L^2-approximation property if

$$\|h_Y^{-1}(v - \Pi v)\|_{L^2(\Omega_Y)} \lesssim |v|_{H^1(\Omega_X)}, \quad \forall\, v \in X. \tag{1.2}$$

Here and in the following, we write $a \lesssim b$ if there is a constant c, which is independent of the meshes, particularly of h_Y in (1.1) and (1.2), and the considered functions,

such that $a \leq cb$. Note that no relation between X and Y has been specified other than the fact that functions from X are also well-defined in the domain Ω_Y. Definition 1.1 constitutes a quite general but common concept; the notions are used for both coarse-to-fine and fine-to-coarse operators. The term H^1-stability is slightly stronger than H^1-continuity, especially in the finite-dimensional case where every linear operator is continuous (with respect to every equivalent norm), because the latter notion includes mappings with a continuity constant dependent on the mesh.

A direct consequence of the L^2-approximation property (1.2) is that $\|v - \Pi v\|_{L^2(\Omega_Y)} \to 0$ for $\|h_Y\|_{L^\infty(\Omega_Y)} \to 0$, which holds for all $v \in X$. This observation, which has already been considered by Clément in his work [26] on finite element interpolation of non-smooth functions, further illustrates the nature of the operators addressed in this paper: An approximation operator mapping to a finite element space converges (with respect to the L^2-norm) to the natural embedding for increasing dimension of the target space.

Definition 1.2. *Let Y be a finite element space associated with a mesh of a domain Ω_Y with nodes $\mathcal{N}_Y$, $n_Y := |\mathcal{N}_Y|$, and coordinate isomorphism $\Phi_Y : \mathbb{R}^{n_Y} \to Y$. An operator $\Pi_Y : H^1(\Omega_Y) \to Y$ is called local if*

$$\big(\Phi_Y^{-1}(\Pi_Y v)\big)_p = \big(\Phi_Y^{-1}(\Pi_Y w)\big)_p, \quad \forall\, p \in \mathcal{N}_Y,\ \forall\, v,\, w \in H^1(\Omega_Y),\ v|_{\omega_p} = w|_{\omega_p}.$$

In this paper, we discuss both non-local (global) and local operators in the sense of Definition 1.2. Note that, indeed, the patch ω_p is generally the most reasonable "domain of influence" of the value at node p for the construction of a local approximation operator.

Finally, consider the case that an operator $\Pi_\ell : H^1(\Omega_\ell) \to X_\ell$ acts as the identity mapping on the target space. This is true if, for instance, Π_ℓ is a surjective projection. Then, if the meshes $\mathcal{T}_{\ell-1}$ and $\mathcal{T}_\ell$ are nested, the fact that the corresponding spaces $X_{\ell-1} \subset X_\ell$ are also nested implies immediately that the restricted mapping $\Pi_{\ell-1}^\ell : X_{\ell-1} \to X_\ell$ is the natural embedding. This is a desirable property because one might argue that otherwise (if there exists an element $v \in X_{\ell-1}$ such that $\Pi_\ell \Pi_\ell v \neq \Pi_\ell v$) a considerable part of structure (namely the appreciable fact that $X_{\ell-1} \subset X_\ell$) is unnecessarily disregarded.

2. Operators between finite element spaces associated with non-nested meshes

In this section, we present various transfer operators and review their fundamental properties. Both intuitive and more elaborate mappings are examined to understand the information transfer between finite element spaces associated with non-nested meshes. We discuss locally and globally defined operators including well-known quasi-interpolation concepts and also focus on their algorithmic structure. Each transfer operator is at least "geometrically inspired", namely the algorithm to compute a concrete

realization incorporates geometric information in terms of finite element meshes. All operators presented here are studied experimentally in Section 3 and Section 4.

2.1. Standard finite element interpolation

First, we consider the most elementary operator. The standard finite element interpolation or nodal interpolation in case of first order Lagrange elements is defined by

$$\mathcal{I}_\ell : \mathcal{C}^0(\Omega) \to X_\ell, \quad u \mapsto \mathcal{I}_\ell u := \sum\nolimits_{p\in\mathcal{N}_\ell} u(p)\lambda_p^\ell.$$

Here and in the following, assume that the generic domain Ω is sufficiently large. The operator is surjective, namely $\mathcal{I}_\ell(\mathcal{C}^0(\Omega)) = X_\ell$, and a projection, i.e., for every $v \in \mathcal{C}^0(\Omega)$ we have $\mathcal{I}_\ell\mathcal{I}_\ell v = \mathcal{I}_\ell v$. The interpolation in X_ℓ with the domain restricted to the finite element space $X_{\ell-1}$ is called $\mathcal{I}_{\ell-1}^\ell$. Evidently, the operator is local according to Definition 1.2. Moreover, when restricted to finite element spaces, it possesses the H^1-stability and L^2-approximation properties given in Definition 1.1 for shape regular meshes. This result can be found in several papers; see, e.g., [20, 24, 58]. For counterexamples for general H^1-functions and $d = 2$, see [3].

From a computational point of view, the standard nodal interpolation is very attractive. Given an arbitrary function in $\mathcal{C}^0(\Omega)$, the computation of the interpolant is very cheap with one function evaluation per node in $\mathcal{N}_\ell$, i.e., per basis function in Λ_ℓ. It is without any doubt the least expensive way to transfer information to a finite element space in a reasonable way. For the computation of the matrix representation in $\mathbb{R}^{n_\ell\times n_{\ell-1}}$, this amounts to the evaluation of $\lambda_q^{\ell-1}(p)$ for all $q \in \mathcal{N}_{\ell-1}$ and $p \in \mathcal{N}_\ell$. Naturally, one may neglect the combinations with $p \notin \omega_q$. This is straightforward if successive meshes are nested and parent-child relations are known. In the non-nested setting, such neighborhood relations have to be computed; see Section 2.6.

On the H^1-stability of the nodal interpolation

In the literature, several different proofs have been brought forth for the stability and approximation property of the nodal interpolation in case the domain is restricted to a (coarser) finite element space; see [20, 24, 58]. The stability estimates usually depend on the shape regularity of the meshes which, in general, leads to constants greater than one. However, we found an elementary proof in case $d = 1$, where no shape regularity assumption needs to be considered, for the fact that "interpolation smoothes". The following lemma states for the one-dimensional setting that the linear interpolation operator $\mathcal{I}_{\ell-1}^\ell : X_{\ell-1} \to X_\ell$ has an H^1-stability constant less than or equal to one whether or not Dirichlet conditions come into play. The uniform estimates hold without any assumptions on the mesh sizes or on the relations between the meshes.

Lemma 2.1. *Let $d = 1$. Then, the nodal interpolation operator $\mathcal{I}_{\ell-1}^\ell : X_{\ell-1} \to X_\ell$ satisfies the following uniform H^1-stability estimates:*

If $\Omega_\ell \subset \Omega_{\ell-1}$,

$$|\mathcal{I}_{\ell-1}^{\ell} v|_{H^1(\Omega_\ell)} \leq |v|_{H^1(\Omega_\ell)} \leq |v|_{H^1(\Omega_{\ell-1})}, \quad \forall\, v \in X_{\ell-1},$$

otherwise,

$$|\mathcal{I}_{\ell-1}^{\ell} \mathcal{E}\, v|_{H^1(\Omega_\ell)} \leq |v|_{H^1(\Omega_\ell \cap \Omega_{\ell-1})}, \quad \forall\, v \in X_{\ell-1},\ v|_{\partial\Omega_{\ell-1}} = 0,$$

where $\mathcal{E} : H_0^1(\Omega_{\ell-1}) \to H^1(\Omega_{\ell-1} \cup \Omega_\ell)$ *is the natural extension by zero. Moreover, the interpolation operator* $\mathcal{I}_{\ell-1}^{\ell,0} : X_{\ell-1} \to X_\ell \cap H_0^1(\Omega_\ell)$ *enforcing zero function values at* $\partial\Omega_\ell$ *satisfies*

$$|\mathcal{I}_{\ell-1}^{\ell,0} \mathcal{E}\, v|_{H^1(\Omega_\ell)} \leq |v|_{H^1(\Omega_\ell \cap \Omega_{\ell-1})}, \quad \forall\, v \in X_{\ell-1},\ v|_{\partial\Omega_{\ell-1}} = 0,\ v|_{\partial\Omega_\ell \cap \overline{\Omega}_{\ell-1}} = 0.$$

We emphasize that the symbols $\subset$ and $\supset$ always include the case of equality. The proof and more details are elaborated in [31]. There, we also give counterexamples for the nodal interpolation in higher order finite element spaces. For stability and approximation properties with respect to the L^∞-norm, see, e.g., [19].

2.2. Clément-type quasi-interpolation

The following class of approximation operators has originally been introduced in [26] to generalize the nodal interpolation in finite element spaces if the considered functions are discontinuous. Quasi-interpolation is probably most famous for its frequent usage in proofs of the reliability of a posteriori error estimators; see [23, 60] for a detailed review.

The Clément operator is defined by

$$\mathcal{R}_\ell : L^2(\Omega) \to X_\ell, \quad u \mapsto \mathcal{R}_\ell u := \sum\nolimits_{p \in \mathcal{N}_\ell} (Q_p u)(p) \lambda_p^\ell, \tag{2.1}$$

with the L^2-projections Q_p onto the local polynomial spaces $\mathbb{P}_r(\omega_p)$ of degree $r \in \mathbb{N}$, i.e.,

$$u \mapsto Q_p u \in \mathbb{P}_r(\omega_p) : \quad (Q_p u, v)_{L^2(\omega_p)} = (u, v)_{L^2(\omega_p)}, \quad \forall\, v \in \mathbb{P}_r(\omega_p),\ p \in \mathcal{N}_\ell. \tag{2.2}$$

For instance, each projection Q_p simply acts as local averaging by $Q_p u = \frac{1}{|\omega_p|} \int_{\omega_p} u \, d\boldsymbol{x}$ if $r = 0$. By construction, the generated operators are local according to Definition 1.2.

Lemma 2.2 ([4, 12, 26])**.** *The Clément operator* $\mathcal{R}_\ell$ *is* H^1*-stable and has the* L^2*-approximation property for* $r \in \mathbb{N}$.

Whereas the original results in [26] have been derived for triangular meshes in case $d = 2$, the relevant properties can indeed be proved for finite element spaces associated with general, not necessarily affine meshes and $d \in \{2, 3\}$. Note that the assertion holds true for non-quasi-uniform meshes; we refer the reader to the discussion in [4]. The

technical ideas of the proof are perhaps most clearly elaborated in [12, Lemma 3.1], although in a slightly different context.

By definition, the Clément interpolation acts as the nodal interpolation on polynomials of degree r, namely $\mathcal{R}_\ell v = \mathcal{I}_\ell v$ for all $v \in \mathbb{P}_r(\Omega)$. For the purpose of information transfer between finite element spaces, regardless of whether nested or non-nested, which are built from piecewise polynomials, this cannot be exploited, though.

Restricting the attention to the discrete space X_ℓ, one notes that the Clément interpolation $\mathcal{R}_\ell : X_\ell \to X_\ell$ does not keep invariant the basis functions; see (2.3) below. But this information is not sufficient to determine the projection properties of the operator in the spaces $L^2(\Omega)$ and $X_{\ell-1}$, respectively. This is because, in general, one does not know whether the functions $\lambda_p^\ell \in \Lambda_\ell$ are contained in the range $\mathcal{R}_\ell(L^2(\Omega))$ or even $\mathcal{R}_\ell(X_{\ell-1})$. However, considering the size of the supports of the images of certain functions, we can prove the following

Proposition 2.1. *Let the mesh $\mathcal{T}_\ell$ contain at least two interior nodes. Then, the quasi-interpolation $\mathcal{R}_\ell : L^2(\Omega) \to X_\ell$ is not a projection.*

Proof. Let $v \in L^2(\Omega)$ be a non-negative, non-trivial function such that $\operatorname{supp}(\mathcal{R}_\ell v) \neq \overline{\Omega}$. It is easy to see that such a "local" function v exists if the mesh $\mathcal{T}_\ell$ has at least two interior nodes. Then, one can find an element $T_0 \in \mathcal{T}_\ell$ with $T_0 \not\subset \operatorname{supp}(\mathcal{R}_\ell v)$ but $\overline{T}_0 \cap \operatorname{supp}(\mathcal{R}_\ell v) \neq \emptyset$, in other words an element adjacent to the support of $\mathcal{R}_\ell v$. It is obvious that

$$\operatorname{supp}(\mathcal{R}_\ell \lambda_p^\ell) = \bigcup \left\{ \overline{T} \mid T \in \mathcal{T}_\ell,\, \overline{T} \cap \omega_p \neq \emptyset \right\}, \quad \forall\, p \in \mathcal{N}_\ell. \tag{2.3}$$

By definition, we have the linear combination $\mathcal{R}_\ell \mathcal{R}_\ell v = \sum_{p \in \mathcal{N}_\ell} (Q_p v)(p) \mathcal{R}_\ell \lambda_p^\ell$ with numbers $(Q_p v)(p) \geq 0$. Because the functions $\mathcal{R}_\ell \lambda_p^\ell = \sum_{r \in \mathcal{N}_\ell} (Q_r \lambda_p^\ell)(r) \lambda_r^\ell$, $p \in \mathcal{N}_\ell$, are also non-negative, the contributions coming from $\mathcal{R}_\ell \lambda_p^\ell$ and $\mathcal{R}_\ell \lambda_q^\ell$, $p \neq q$, do not cancel out each other in the calculation of the effective coefficients of $\mathcal{R}_\ell \mathcal{R}_\ell v$ with respect to the basis Λ_ℓ. Thus, it follows that $T_0 \subset \operatorname{supp}(\mathcal{R}_\ell \mathcal{R}_\ell v)$ and, consequently, $\mathcal{R}_\ell \mathcal{R}_\ell v \neq \mathcal{R}_\ell v$. This concludes the proof of the proposition. □

There are in fact subspaces $U \subset L^2(\Omega)$ such that $\mathcal{R}_\ell \mathcal{R}_\ell u = \mathcal{R}_\ell u$ for all $u \in U$; for instance, $\mathbb{P}_r(\Omega)$ has this property, as mentioned before. We now investigate to what extent the above considerations also hold true for $\mathcal{R}_{\ell-1}^\ell : X_{\ell-1} \to X_\ell$, namely if the domain of the operator is restricted to the discrete subspace $X_{\ell-1}$. For this purpose, suppose that there is a node $p \in \mathcal{N}_{\ell-1}$ and an element $T_1 \in \mathcal{T}_\ell$ such that

$$\operatorname{int}\left(\bigcup \{ \overline{T} \mid T \in \mathcal{T}_\ell,\, T \cap \operatorname{supp}(\lambda_p^{\ell-1}) \neq \emptyset \} \right) \cap \operatorname{int}\left(\bigcup \{ \overline{T} \mid T \in \mathcal{T}_\ell,\, \overline{T} \cap \overline{T}_1 \neq \emptyset \} \right) = \emptyset. \tag{2.4}$$

Simply put, T_1 needs to be sufficiently far away from the "reach of p". This implies that $\operatorname{int}(\operatorname{supp}(\mathcal{R}_\ell \lambda_p^{\ell-1})) \cap T_1 = \emptyset$. Thus, $\operatorname{supp}(\mathcal{R}_\ell \lambda_p^{\ell-1}) \neq \overline{\Omega}$ and one can find an element $T_0 \in \mathcal{T}_\ell$ which is adjacent to the support of $\mathcal{R}_\ell \lambda_p^{\ell-1}$. Concluding as before, we have the following:

Proposition 2.2. *Provided that* (2.4) *can be fulfilled, the Clément interpolation is not a projection even if its domain is restricted to the discrete subspace* $X_{\ell-1}$.

Note that the relatively weak assumption (2.4) is valid for virtually every pair of meshes $(\mathcal{T}_{\ell-1}, \mathcal{T}_\ell)$ one might handle. Therefore, we have shown that the Clément interpolation operator is practically never a projection.

From Proposition 2.2 we observe the following: Neither does the Clément operator reduce to the standard interpolation in case of nested meshes $\mathcal{T}_{\ell-1}$ and $\mathcal{T}_\ell$ nor is it the identity mapping if the meshes and hence the associated spaces are identical. Evidently, this observation is valid for any polynomial degree $r \in \mathbb{N}$. In addition, this deficiency cannot be overcome by changing the local domains $(\omega_p)_{p\in\mathcal{N}_\ell}$ in (2.2) by introducing another type of (overlapping or non-overlapping) decomposition of local neighborhoods. One could, however, turn the quasi-interpolation into a projection by choosing a suitable restriction of the original finite element space as local space.

2.3. The L^2-projection

In this section, we comment on the use of an operator which appears naturally in the present context. Let $\mathcal{Q}_\ell : L^2(\Omega) \to X_\ell$ be the L^2-projection onto X_ℓ, i.e., the orthogonal projection in the Hilbert space $L^2(\Omega)$ to the subspace X_ℓ characterized by the variational equation

$$u \mapsto \mathcal{Q}_\ell u \in X_\ell : \quad (\mathcal{Q}_\ell u, v)_{L^2(\Omega)} = (u, v)_{L^2(\Omega)}, \quad \forall\, v \in X_\ell.$$

The mapping $\mathcal{Q}_\ell$ is global as opposed to Definition 1.2. This can be understood considering the algebraic representation of the fully discrete operator $\mathcal{Q}_{\ell-1}^\ell$ via a product

$$\mathcal{Q}_{\ell-1}^\ell v = \Phi_\ell(\boldsymbol{M}_\ell^{-1}\boldsymbol{B}_\ell\Phi_{\ell-1}^{-1}(v)), \quad \forall\, v \in X_{\ell-1}, \tag{2.5}$$

with the mass matrix $\boldsymbol{M}_\ell \in \mathbb{R}^{n_\ell\times n_\ell}$ with respect to Λ_ℓ, i.e., $(\boldsymbol{M}_\ell)_{pq} = (\lambda_p^\ell, \lambda_q^\ell)_{L^2(\Omega)}$ for $p, q \in \mathcal{N}_\ell$, and a sparse coupling matrix $\boldsymbol{B}_\ell \in \mathbb{R}^{n_\ell\times n_{\ell-1}}$ with the entries

$$(\boldsymbol{B}_\ell)_{pq} = (\lambda_p^\ell, \lambda_q^{\ell-1})_{L^2(\Omega)}, \quad \forall\, p \in \mathcal{N}_\ell,\ q \in \mathcal{N}_{\ell-1}. \tag{2.6}$$

Therefore, the L^2-projection "as is" cannot be expected to yield a computationally efficient information transfer unless the evaluation of $\boldsymbol{M}_\ell^{-1}$ can be avoided. Note that the operator attained by simply lumping the matrix $\boldsymbol{M}_\ell$ is considered in Section 2.4. We emphasize that some of the (to a greater or lesser extent sophisticated) operators discussed in the literature and in this paper are distinctly motivated by the idea to find an L^2-projection-like mapping or a weighted interpolation which is more suitable for computations.

To obtain a stability estimate for the L^2-projection, the requirement of quasi-uniformity of the mesh $\mathcal{T}_\ell$ has been considered inevitable for quite a long time. Meanwhile, weaker criteria ensuring the H^1-stability of $\mathcal{Q}_\ell$ are available; see, e.g. [12, 22, 28, 56]. For estimates with respect to other Lebesgue norms, see [34] and the

references therein. Two different proofs both using inverse estimates of Bernstein-type, which generally hold true only for quasi-uniform meshes, can be found in [16, Theorem 3.4] and [10, Folgerung II.7.8]. The L^2-approximation property in case of quasi-uniform meshes can be proved with elementary techniques employing another suitable approximation operator such as the Clément quasi-interpolation. In contrast, for a direct proof, see, e.g., [16, Theorem 3.2]. The latter employs the fact that $\mathcal{Q}_\ell$ yields the best approximation in X_ℓ with respect to the norm $\|\cdot\|_{L^2(\Omega)}$. Further ingredients are a standard finite element interpolation error estimate and an interpolation technique between Sobolev spaces.

2.4. On L^2-quasi-projections

In this section, we consider a concept from the literature yielding local approximation operators. The following quasi-projection operator has been employed in [13] to approximate the L^2-projection from the space $H^1(\Omega)$ to the discrete spaces X_ℓ. It is a mapping directly defined via the formula

$$\widetilde{\mathcal{Q}}_\ell : L^2(\Omega) \to X_\ell, \quad u \mapsto \widetilde{\mathcal{Q}}_\ell u := \sum\nolimits_{p\in\mathcal{N}_\ell} \frac{(\lambda_p^\ell, u)_{L^2(\Omega)}}{(\lambda_p^\ell, \mathbb{1})_{L^2(\Omega)}} \lambda_p^\ell, \tag{2.7}$$

where $\mathbb{1}$ denotes the constant function with value 1; see also [21]. After all, we can obtain a matrix representation of the fully discrete operator $\widetilde{\mathcal{Q}}_{\ell-1}^\ell : X_{\ell-1} \to X_\ell$ from the one of the standard L^2-projection in a simple way by lumping the mass matrix $\boldsymbol{M}_\ell$ in (2.5). In the numerical practice, this seems a very natural thing to do. Moreover, for simplicial meshes, it is easy to verify by integration over the reference element that $(\lambda_p^\ell, \mathbb{1})_{L^2(\Omega)} = |\omega_p|/(d+1)$ for all $p \in \mathcal{N}_\ell$; thus, the operator $\widetilde{\mathcal{Q}}_\ell$ may equivalently be defined by the variational equation

$$u \mapsto \widetilde{\mathcal{Q}}_\ell u : \quad (\widetilde{\mathcal{Q}}_\ell u, v)_\ell = (u, v)_{L^2(\Omega)}, \quad \forall\, v \in X_\ell, \tag{2.8}$$

with a specific discrete inner product $(\cdot,\cdot)_\ell$ in X_ℓ, namely

$$(u, v)_\ell := \frac{1}{d+1} \sum\nolimits_{T\in\mathcal{T}_\ell} |T| \sum\nolimits_{p\in\mathcal{N}_\ell\cap\overline{T}} u(p)v(p), \quad \forall\, u, v \in X_\ell, \tag{2.9}$$

as proposed, e.g., in [64]. In other words, $\widetilde{\mathcal{Q}}_\ell$ is the orthogonal projection to the space X_ℓ equipped with $(\cdot,\cdot)_\ell$. Another discrete inner product also motivated by a quadrature rule (on centroids of faces instead of nodes) can be found in [11]. There, it is used in the fashion of (2.8) to define a prolongation operator between the non-nested spaces associated with a discretization with Crouzeix-Raviart elements on nested meshes.

Note that $\widetilde{\mathcal{Q}}_\ell$ is usually not a projection; this motivates the term quasi-projection. A proof of this assertion can be achieved analogously to the ones of Proposition 2.1 and Proposition 2.2, which treat the same issue for the Clément interpolation. In addition, one can easily see that for $p \in \mathcal{N}_\ell$ we have $(\lambda_p^\ell, \lambda_p^\ell)_{L^2(\Omega)} < (\lambda_p^\ell, \mathbb{1})_{L^2(\Omega)}$; thus, $\widetilde{\mathcal{Q}}_\ell \lambda_p^\ell \neq \lambda_p^\ell$.

One needs to notice that there is virtually no experience with quasi-projections in practical computations. However, proofs of the H^1-stability and the L^2-approximation property of the operators $\widetilde{\mathcal{Q}}_\ell$ for shape regular families of meshes are derived by well-known arguments as described at the end of Section 2.5.

Finally, we notice that $\widetilde{\mathcal{Q}}_\ell$ is self-adjoint with respect to the L^2-inner product, i.e.,

$$(\widetilde{\mathcal{Q}}_\ell u, v)_{L^2(\Omega)} = \sum\nolimits_{p\in\mathcal{N}_\ell} \frac{(\lambda_p^\ell, u)_{L^2(\Omega)}(\lambda_p^\ell, v)_{L^2(\Omega)}}{(\lambda_p^\ell, \mathbb{1})_{L^2(\Omega)}} = (u, \widetilde{\mathcal{Q}}_\ell v)_{L^2(\Omega)}, \quad \forall\, u, v \in L^2(\Omega).$$

However, we do not know whether this property may be put to a good use in the analysis or the practical computations at this point. This is because the two involved spaces are usually not identical in applications. Note that the only operator that is self-adjoint and at the same time a projection is the orthogonal projection $\mathcal{Q}_\ell$.

2.5. The pseudo-L^2-projection

In this section, a transfer operator is considered which is different in some respects. It will be denoted by the symbol $\mathcal{P}$ with the appropriate indices. Generally speaking, we introduce a Petrov-Galerkin scheme with a discontinuous test space built from a set of functions which are biorthogonal to the standard nodal basis with respect to the L^2-inner product $(\cdot,\cdot)_{L^2(\Omega)}$. By this means, the global variational formulation defines local mappings, which is similar to (2.8). In the fully discrete setting, this yields a band matrix representation of the operator as no mass matrix has to be inverted.

The mapping $\mathcal{P}_\ell$ is in fact a projection from $L^2(\Omega)$ onto the finite element space X_ℓ. Additionally, in the authors' view, the operator represents a way to get "as close as possible" to the real L^2-projection while at the same time it guarantees an efficient evaluation. This is clearly confirmed by the numerical experiments in Section 3 and Section 4. Therefore, we suggest to call this oblique projection operator "pseudo-L^2-projection" in this context. This term is also meant to contrast, e.g., the L^2-quasi-projection concepts of Section 2.4, which yield in actual fact no projections. Moreover, the pseudo-L^2-projection seems to be the only, reasonably straightforward operator in the fashion of the previous ones (2.7) and (2.8) which is actually a projection.

For the definition of the operator, choose a set of functions $\Psi_\ell = (\psi_p^\ell)_{p\in\mathcal{N}_\ell}$ with $\psi_p^\ell|_{\omega_p} \in \mathcal{C}^0(\omega_p)$ for all $p \in \mathcal{N}_\ell$, extended to Ω by zero, such that

$$(\psi_p^\ell, \lambda_q^\ell)_{L^2(\Omega)} = \delta_{pq}(\lambda_p^\ell, \mathbb{1})_{L^2(\Omega)}, \quad \forall\, p, q \in \mathcal{N}_\ell, \tag{2.10}$$

and set the discontinuous test space as $Y_\ell := \operatorname{span}\{\psi_p^\ell \,|\, p \in \mathcal{N}_\ell\} \not\subset \mathcal{C}^0(\Omega)$. Note that such a dual basis with respect to $(\cdot,\cdot)_{L^2(\Omega)}$ of the nodal finite element basis $\Lambda_\ell = (\lambda_p^\ell)_{p\in\mathcal{N}_\ell}$ exists. This can also be seen, for example, in the various procedures in [37, 49] for an explicit construction of the set Ψ_ℓ. In particular, on its support ω_p, each ψ_p^ℓ can be represented by a linear combination of the nodal basis functions associated with the adjacent elements restricted to ω_p. In case of affine elements, the coefficients do not depend on the actual node p and element T but can be computed on the reference

element in a one-time process; no inverse element mass matrices are necessary. This is due to the scaling with $(\lambda_p^\ell, \mathbb{1})_{L^2(\Omega)}$ on the right hand side of (2.10) which also implies the boundedness $\|\psi_p^\ell\|_{L^\infty(\Omega)} \lesssim 1$ for all $p \in \mathcal{N}_\ell$. For a more detailed analysis of biorthogonal bases, carried out in the context of the mortar finite element method [9], and the construction of such systems for higher order finite element spaces, we refer to [41, 43, 44, 63].

Now, we define the pseudo-L^2-projection $\mathcal{P}_\ell : L^2(\Omega) \to X_\ell$ by a global Petrov-Galerkin variational formulation with trial space X_ℓ and test space Y_ℓ, i.e.,

$$u \mapsto \mathcal{P}_\ell u : \quad (\mathcal{P}_\ell u, v)_{L^2(\Omega)} = (u, v)_{L^2(\Omega)}, \quad \forall\, v \in Y_\ell. \tag{2.11}$$

This variational problem has a unique solution because $\dim(Y_\ell) = \dim(X_\ell) < \infty$ and for $u \in X_\ell$ it is $(u, v)_{L^2(\Omega)} = 0$ for all $v \in Y_\ell$ if and only if $u = 0$. In particular, the definition yields the obvious representation formula

$$\mathcal{P}_\ell u = \sum\nolimits_{p \in \mathcal{N}_\ell} \frac{(\psi_p^\ell, u)_{L^2(\Omega)}}{(\lambda_p^\ell, \mathbb{1})_{L^2(\Omega)}} \lambda_p^\ell, \quad \forall\, u \in L^2(\Omega). \tag{2.12}$$

The operator $\mathcal{P}_\ell$ is well-defined by Hölder's inequality. The fully discrete representation in $\mathbb{R}^{n_\ell \times n_{\ell-1}}$ of the pseudo-L^2-projection $\mathcal{P}_{\ell-1}^\ell : X_{\ell-1} \to X_\ell$ is obtained analogously to the ones of the L^2-projection and the L^2-quasi-projection from the previous sections.

The idea to use a Petrov-Galerkin scheme to define a generalized projection operator can be found in [56] for $d \in \{1, 2\}$, too. There, the test space is constructed differently; the local test functions are associated with a dual mesh. Undoubtedly, the root of the considered operators lies in the research of quasi-interpolation concepts by Clément [26]. However, the first appearance of a weighted interpolation operator using a system of biorthogonal test functions was in [54]. Biorthogonal systems of some form or another are classic in linear algebra and considerably more common in the context of wavelets; see, e.g., [27, 29, 61]. Generalized projections using dual test functions have first been introduced to the area of domain decomposition methods by [62, 63] and then [41]. In practical computations, operators of this type have been used to map trace functions between non-matching interfaces; see also [32, 33] and the references therein.

As opposed to the earlier version proposed in [54], we do not aspire to preserve Dirichlet boundary conditions on $\partial\Omega$. This is immediately reflected by the definition as $\operatorname{supp}(\psi_p^\ell) = \omega_p$ also for boundary nodes. We do not have to choose suitable $(d-1)$-dimensional sub-simplices on the boundary but rather work with the given finite element meshes, which makes the definition, in a sense, more symmetric. A further advantage, which we do not yet exploit here, is the lower requirement for the regularity of the considered functions, namely $L^1(\Omega)$ instead of $W_p^m(\Omega)$ with $m \geq 1$ if $p = 1$ and $m > 1/p$ otherwise; see also [21].

Let us now examine the properties of the operator more closely. First of all, the mapping $\mathcal{P}_\ell$ is surjective, namely $\mathcal{P}_\ell(L^2(\Omega)) = X_\ell$, because (2.10) and (2.12) immediately imply $\mathcal{P}_\ell \lambda_p^\ell = \lambda_p^\ell$ for all $p \in \mathcal{N}_\ell$. Moreover, it is a projection onto X_ℓ. This is

a simple consequence of the linearity of the operator and, again, the biorthogonality property (2.10). In addition, it is important to note the following:

Lemma 2.3. *The pseudo-L^2-projection $\mathcal{P}_\ell$ is H^1-stable and has the L^2-approximation property for all shape regular families of meshes.*

The assertion may proved by well-known arguments as Poincaré's inequality and the fact that constant functions are reproduced locally; see [30, Section 5.5]. It indeed holds true for shape regular (not necessarily quasi-uniform) meshes with a mesh size function $h_\ell \in L^\infty_>(\Omega)$ because all estimates are local; in an element $T \in \mathcal{T}_\ell$ they only involve the values in a small neighborhood. Similar arguments yield the H^1-stability and the L^2-approximation property of the L^2-quasi-projection $\widetilde{\mathcal{Q}}_\ell$ described in Section 2.4 as it also reproduces the constant functions locally.

2.6. Implementation aspects

In this section, we focus on the realization of the specific transfer operators in practical finite element codes. All described methods are implemented in a module `nnmglib` (developed in [30]) in the package `obslib++`, which is maintained by the second author and his work group. The software uses fundamental components of the finite element toolbox `ug`; see [7].

For the computation of a matrix representation of a linear operator from $X_{\ell-1}$ to X_ℓ, one needs to deal with quantities associated with different meshes without any usable a priori relation. Therefore, we have incorporated the quadtree/octree implementation of [2] into `obslib++`. Suitable advancing front techniques exploiting the connectivities of the single meshes can be applied instead; see, e.g., [38] in a related context. In any case, for each node $p \in \mathcal{N}_\ell$, a set $\mathcal{N}_{\ell-1}^p \subset \mathcal{N}_{\ell-1}$ containing a sufficiently small number of nodes is determined such that

$$q \in \mathcal{N}_{\ell-1}, \;\; \operatorname{int}(\omega_q) \cap \operatorname{int}(\omega_p) \neq \emptyset \implies q \in \mathcal{N}_{\ell-1}^p.$$

Then, all terms which appear in the presented discrete operators may evidently be computed only based on these local index subsets. This results in almost linear complexity of the assembly procedure.

2.6.1. Numerical integration

For all transfer operators, with the exception of the nodal interpolation, L^2-inner products of functions associated with different meshes need to be computed. This is obvious for the operators $\mathcal{Q}_{\ell-1}^\ell$ and $\widetilde{\mathcal{Q}}_{\ell-1}^\ell$ involving the sparse but global coupling matrix $\boldsymbol{B}_\ell \in \mathbb{R}^{n_\ell \times n_{\ell-1}}$ defined in (2.6). The analogon for the pseudo-L^2-projection $\mathcal{P}_{\ell-1}^\ell$ requires the entries

$$(\psi_p^\ell, \lambda_q^{\ell-1})_{L^2(\omega_p \cap \omega_q)}, \quad \forall\, p \in \mathcal{N}_\ell,\; q \in \mathcal{N}_{\ell-1}. \tag{2.13}$$

We turn to the other mappings which employ local orthogonal projections below.

To evaluate (2.6) or (2.13) exactly, one has to compute the intersections of the elements in the consecutive meshes. As we have previously done in [32] for the intersection of locally projected non-matching interface meshes, we employ the quickhull algorithm in an implementation by [6] for this purpose. After a suitable remeshing of the computed intersection polytopes, one achieves an exact integration, up to roundoff errors, by the application of low order quadrature rules. We have implemented the methods concerning element intersections in a module `cutlib`.

In practice, good results may be obtained by an approximate numerical integration via a quadrature rule solely based on the finer mesh. The order of the employed quadrature rules should be adequate such that they are exact at least in case of nested meshes. This requires order two for the above operators and order $r+1$ for the Clément quasi-interpolations. We are aware of the fact that such an approach might fail to retain optimal (discretization) error estimates, for instance, in the mortar finite element setting; see [36, 45]. However, let us refer to the numerical studies in Section 3.3, where we demonstrate that the error in the operator itself due to approximate integration is small if the quadrature rule is chosen adequately.

2.6.2. Computation of orthogonal projections

The evaluation of the operator $\mathcal{Q}_{\ell-1}^{\ell}$, which is the orthogonal projection to the space X_ℓ with respect to the L^2-inner product, is very expensive. For the experiments in Section 3 and Section 4, we employ the direct sparse solver `pardiso` [52, 53] to decompose the appearing mass matrices. This is more efficient than an iterative solver in this special case as the respective inverse needs to be applied to a large number of vectors. The pseudo-L^2-projection $\mathcal{P}_{\ell-1}^{\ell}$ is also defined via a global variational formulation but can be evaluated efficiently by construction. Note that the quasi-projection $\widetilde{\mathcal{Q}}_{\ell-1}^{\ell}$ yields a simple formulation, too. The same holds true for a quasi-interpolation operator in case the local trial and test spaces are one-dimensional, e.g., for the Clément operator $\mathcal{R}_{\ell-1}^{\ell}$ with $r = 0$.

In contrast, we have seen that general transfer operators may require the evaluation of local orthogonal projections. In the following, we sketch the implementation of the operators $\mathcal{R}_{\ell-1}^{\ell}$ with $r > 0$. To solve the corresponding local variational equations (2.2) for the right hand sides given by the coarse level basis functions, one needs to compute coarse-to-fine coupling matrices and mass matrices similar to the ones in (2.5) but associated with the local spaces. Let $(\phi_i^p)_{1\le i\le n_p}$ be a basis of the considered trial space at $p \in \mathcal{N}_\ell$. Then,

$$(\boldsymbol{M}_p)_{ij} = (\phi_i^p, \phi_j^p)_{L^2(\omega_p)}, \quad \forall\, 1 \le i, j \le n_p,$$

and

$$(\boldsymbol{B}_p)_{iq} = (\phi_i^p, \lambda_q^{\ell-1})_{L^2(\omega_p)}, \quad \forall\, 1 \le i \le n_p,\ q \in \mathcal{N}_{\ell-1}, \tag{2.14}$$

are the respective local matrices. We omit the level index ℓ as it is clear from the choice of p. For the Clément quasi-interpolation operators, the trial and test spaces are obtained by restrictions of global polynomial spaces to the patches. Therefore, one

may choose a universal basis for the implementation; for instance, $(\phi_i)_{1\leq i\leq d+1}$ with $\phi_i(\boldsymbol{x}) = \boldsymbol{x}\cdot\boldsymbol{e}_i$ for $1\leq i\leq d$ and $\phi_{d+1}\equiv 1$ is a convenient choice in case $r=1$. The issues concerning the numerical integration of (2.14) are solved as before for the global coupling matrices. As usual in finite element assembly algorithms, a single loop over all elements in $\mathcal{T}_\ell$ makes sure that no redundant computations are carried out; each integral contribution is only computed once. Finally, the entries of the global matrix representations in $\mathbb{R}^{n_\ell\times n_{\ell-1}}$ of the Clément operators $\mathcal{R}_{\ell-1}^{\ell}: X_{\ell-1}\to X_\ell$ read as

$$\sum\nolimits_{i=1}^{n_p}\sum\nolimits_{j=1}^{n_p}(\boldsymbol{M}_p^{-1})_{ij}(\boldsymbol{B}_p)_{jq}\phi_i(p),\quad \forall\, p\in\mathcal{N}_\ell,\ q\in\mathcal{N}_{\ell-1}.$$

This formula is immediately derived by solving the variational equation (2.2) for the basis functions $(\lambda_q^{\ell-1})_{q\in\mathcal{N}_\ell}$ and evaluating the result at the node p. The inversion of the n_ℓ local mass matrices $(\boldsymbol{M}_p)_{p\in\mathcal{N}_\ell}$ is required with dimension $n_p=\dim(\mathbb{P}_r(\omega_p)) = (d+r)!/(d!\,r!)$.

3. Numerical studies of the diverse transfer operators

Let us now focus on the practical properties of the described transfer operators. In this section, we report on various numerical experiments which are performed to assess interconnections between the single operators. Subjecting the discrete mappings to a close examination, we want to understand better what the fundamental characteristics of the information transfer between non-nested finite element spaces are.

The examples of computational domains studied here are three geometric shapes (ball, cylinder, half torus) each with a series of independently generated meshes; see Section 3.1. To investigate the behaviors of the mappings, we look at suitable operator norms with respect to the L^2-norm and the H^1-semi-norm associated with the appropriate domains. The desired quantities are computed by solving generalized eigenvalue problems as described in Section 3.2. We obtain results on the accuracy of an approximate numerical integration in Section 3.3. Finally, we examine the quantitative differences of the transfer operators by measuring the distances between them in Section 3.4.

The assessment performed here is motivated by the desire to become more familiar with the application of (to a greater or lesser extent sophisticated) (quasi-)interpolation and (quasi-)projection operators in practical computations. It allows for "drawing a map" arranging the operators by their mutual relations. To our knowledge, the evaluation of operators for the information transfer between finite element spaces associated with non-nested meshes has never been studied in such a manner so far.

3.1. Setup of the experiments

For the experiments presented in this section, we consider a number of independently generated meshes of a ball, a cylinder and a half torus, respectively. These are

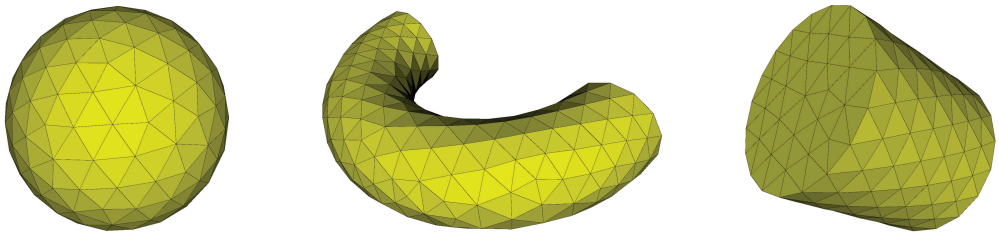

Figure 1: Examples for the unstructured meshes for the numerical studies: ball $\mathcal{B}$, half torus $\mathcal{H}$, cylinder $\mathcal{C}$ (from left to right). The characteristics of the independently generated meshes are given in Table 1.

appropriate geometric settings as one can easily obtain completely independent unstructured volume meshes for a large variety of different mesh sizes by standard tetrahedral mesh generation tools, e.g., from CUBIT [51]. In addition, they yield very good reproducibility. Note that the setting is also sufficiently general. On the one hand, this can be seen in an illustrative example in Remark 3.1 at the beginning of Section 3.4. On the other hand, we study a more complex geometry in Section 4.

We use a set of tetrahedral meshes $(\mathcal{B}_i)_{1\leq i\leq 9}$ of a ball, $(\mathcal{C}_i)_{1\leq i\leq 9}$ of a cylinder and $(\mathcal{H}_i)_{1\leq i\leq 9}$ of a half torus, respectively, with their characteristics given in Table 1 ordered by the number of elements. For each of the geometric shapes, one mesh is illustrated in Fig. 1. Note that the situation between the single meshes is sufficiently general in the sense that there are no mutual relations other than that they approximate the same domain. In particular, none of the meshes stems from a refinement routine; they are all imported separately.

Table 1: Characteristics of the independently generated meshes $(\mathcal{B}_i)_{1\leq i\leq 9}$ of a ball, $(\mathcal{C}_i)_{1\leq i\leq 9}$ of a cylinder and $(\mathcal{H}_i)_{1\leq i\leq 9}$ of a half torus. The meshes do not stem from a refinement routine; they cover a broad range of sizes.

	#elements	#nodes		#elements	#nodes		#elements	#nodes
$\mathcal{B}_1$	292	88	$\mathcal{C}_1$	239	78	$\mathcal{H}_1$	649	191
$\mathcal{B}_2$	580	150	$\mathcal{C}_2$	751	196	$\mathcal{H}_2$	1,421	371
$\mathcal{B}_3$	1,708	392	$\mathcal{C}_3$	1,424	348	$\mathcal{H}_3$	1,964	500
$\mathcal{B}_4$	3,616	778	$\mathcal{C}_4$	4,407	947	$\mathcal{H}_4$	6,392	1,418
$\mathcal{B}_5$	10,711	2,168	$\mathcal{C}_5$	8,100	1,690	$\mathcal{H}_5$	12,329	2,613
$\mathcal{B}_6$	48,320	9,228	$\mathcal{C}_6$	16,591	3,313	$\mathcal{H}_6$	33,486	6,700
$\mathcal{B}_7$	64,773	12,294	$\mathcal{C}_7$	27,681	5,372	$\mathcal{H}_7$	56,959	11,126
$\mathcal{B}_8$	93,620	17,647	$\mathcal{C}_8$	50,195	9,570	$\mathcal{H}_8$	80,881	15,590
$\mathcal{B}_9$	123,946	23,259	$\mathcal{C}_9$	103,746	19,373	$\mathcal{H}_9$	111,439	21,235

For the three cases, we consider mappings between the different meshes and introduce the notations, again, by using the generic operator symbol Π with i and j as indices and exponents. For the purposes of the present section, we do not need to distinguish between the different objects associated with the ball, the cylinder and the half torus by marking the symbols for the domains, spaces and operators, respectively. This is because the geometric shapes are treated one at a time. Consequently, let the

corresponding domains be denoted by $(\Omega_i)_{1\leq i\leq 9}$; accordingly, $(X_i)_{1\leq i\leq 9}$ are the standard finite element spaces associated either with the meshes $(\mathcal{B}_i)_{1\leq i\leq 9}$ or $(\mathcal{C}_i)_{1\leq i\leq 9}$ or $(\mathcal{H}_i)_{1\leq i\leq 9}$ without any boundary modifications. Then, we denote the connecting operators, e.g., by $\Pi_i^j : X_i \to X_j$ for $1 \leq i < j \leq 9$.

3.2. Computation of operator norms

In the following, operator norms play a central role; for $\Pi_i^j, \widetilde{\Pi}_i^j \in \mathrm{Lin}(X_i, X_j)$, we study terms of the form

$$\sup_{v\in X_i\cap H_0^1(\Omega_i),\, \|v\|_i\neq 0} \frac{\|\Pi_i^j v\|_j}{\|v\|_i} \quad \text{or} \quad \sup_{v\in X_i\cap H_0^1(\Omega_i),\, \|v\|_i\neq 0} \frac{\|\Pi_i^j v - \widetilde{\Pi}_i^j v\|_j}{\|v\|_i}, \tag{3.1}$$

where $\|\cdot\|_i$ and $\|\cdot\|_j$ are suitably chosen (semi-)norms in X_i and X_j, respectively. All mentioned transfer operators may be employed to map an infinite-dimensional function space to a finite element space which is normally a subspace. However, we emphasize that we do *not* consider a general Hilbert space setting but restrict the attention to the case of two finite element spaces which is relevant for the outlined applications. Therefore, the suprema in (3.1) are taken over finite element functions in X_i only. Finally, we require the test functions to be in $H_0^1(\Omega_i)$ such that their extensions by zero to the possibly larger domain Ω_j are continuous and piecewise first order polynomials and, thus, weakly differentiable.

To compute quantities of the form (3.1) with respect to the L^2-norm and the H^1-semi-norm, respectively, the corresponding generalized eigenvalue problems are considered. For this purpose, we abbreviate $\mathcal{N}_\ell^0 := \{p \in \mathcal{N}_\ell \mid p \notin \partial\Omega_\ell\}$ and $n_\ell^0 := |\mathcal{N}_\ell^0|$. Let the matrix $\boldsymbol{A}_\ell \in \mathbb{R}^{n_\ell\times n_\ell}$ be the representation of the H^1-semi-norm with respect to Λ_ℓ, i.e., $(\boldsymbol{A}_\ell)_{pq} = \int_{\Omega_\ell} \nabla\lambda_p^\ell \cdot \nabla\lambda_q^\ell \, d\boldsymbol{x}$ for $p, q \in \mathcal{N}_\ell$, and similarly $\boldsymbol{A}_\ell^0 \in \mathbb{R}^{n_\ell^0\times n_\ell^0}$ with entries $(\boldsymbol{A}_\ell^0)_{pq} = \int_{\Omega_\ell} \nabla\lambda_p^\ell \cdot \nabla\lambda_q^\ell \, d\boldsymbol{x}$ for $p, q \in \mathcal{N}_\ell^0$. Naturally, $\boldsymbol{A}_\ell^0$ is symmetric positive definite. We also introduce the mass matrix in the interior $\boldsymbol{M}_\ell^0 \in \mathbb{R}^{n_\ell^0\times n_\ell^0}$ with $(\boldsymbol{M}_\ell^0)_{pq} = (\lambda_p^\ell, \lambda_q^\ell)_{L^2(\Omega_\ell)}$ for $p, q \in \mathcal{N}_\ell^0$. Finally, let $\boldsymbol{\Pi}_i^j \in \mathbb{R}^{n_j\times n_i^0}$ be the matrix representation of an operator $\Pi_i^j : X_i \cap H_0^1(\Omega_i) \to X_j$ with respect to the chosen bases. Then, we have the operator norms

$$\|\Pi_i^j\|_{L^2} = \max\left\{\sqrt{\eta} \in \mathbb{R} \mid \exists\, \boldsymbol{v} \in \mathbb{R}^{n_i^0} \text{ such that } (\boldsymbol{\Pi}_i^j)^T \boldsymbol{M}_j \boldsymbol{\Pi}_i^j \boldsymbol{v} = \eta \boldsymbol{M}_i^0 \boldsymbol{v}\right\} \tag{3.2}$$

and

$$|\Pi_i^j|_{H^1} = \max\left\{\sqrt{\eta} \in \mathbb{R} \mid \exists\, \boldsymbol{v} \in \mathbb{R}^{n_i^0} \text{ such that } (\boldsymbol{\Pi}_i^j)^T \boldsymbol{A}_j \boldsymbol{\Pi}_i^j \boldsymbol{v} = \eta \boldsymbol{A}_i^0 \boldsymbol{v}\right\}. \tag{3.3}$$

For brevity, in the notations of the operator norms, we omit the two different spaces with the two different domains. Distances between operators may be measured likewise by, e.g., $\|\Pi_i^j - \widetilde{\Pi}_i^j\|_{L^2}$ for some $\Pi_i^j, \widetilde{\Pi}_i^j \in \mathrm{Lin}(X_i, X_j)$. We also consider relative

quantities, namely terms of the form $|\Pi_i^j - \widetilde{\Pi}_i^j|_{H^1}/|\Pi_i^j|_{H^1}$. Note that a sampling procedure that we used previously to estimate operator norms yielded essentially the same results.

The generalized eigenvalue problems in (3.2) and (3.3) are solved iteratively by the locally optimal block preconditioned conjugate gradient method (LOBPCG) [42] for the largest eigenvalues. We proceed as outlined in Section 2.6 to obtain numerical representations of the transfer operators. Then, to compute the desired quantities by solving (3.2) and (3.3), respectively, one step of the LOBPCG method requires several matrix-vector multiplications involving mass or stiffness matrices both in $\mathbb{R}^{n_j \times n_j}$ and in $\mathbb{R}^{n_i^0 \times n_i^0}$ as well as prolongation matrices in $\mathbb{R}^{n_j \times n_i^0}$ and their transposes. To evaluate the L^2-projection, additional forward-backward substitutions are necessary.

3.3. Influence of numerical integration

In this section, we consider the inexact integration of the coupling terms between the basis functions of X_i and X_j by means of a quadrature rule solely associated with the target mesh, as described in Section 2.6. We verify that this approximation is very accurate in case of sufficiently many function evaluations per element. (Note that inner products of finite element functions associated with the same mesh are always evaluated exactly except for roundoff errors.) To quantify the effect not on the integrals as such but on the actual mappings, we estimate the relative differences between the transfer operators $\mathcal{Q}$, $\mathcal{P}$, $\widetilde{\mathcal{Q}}$, $\mathcal{R}_{r=0}$, $\mathcal{R}_{r=1}$ and $\mathcal{R}_{r=2}$ on the one hand and approximate versions on the other hand.

For this purpose, composite quadrature formulas are employed. These rules are generated by regular decompositions of the tetrahedron into m^3 tetrahedra of the same volume, $m \in \mathbb{N}_+$. Then, a rule of second order with four points is used on each of the sub-elements. As the integrands are of low order but the integration domains may have relatively complicated shapes, this is an appropriate choice; see Section 2.6.

We look at the decay of the quadrature error for the composite rules with $m = 1, 2, 3$ (that is 4, 32 and 108 points per element, respectively) using the results for $m = 5$ (i.e., 500 points per element) as reference. Fig. 2 shows the relative errors in the evaluation of the transfer operators in logarithmic scale. The results are given for the combinations of the first five meshes of the ball, $(\mathcal{B}_i)_{1\le i\le 5}$, namely we investigate $\Pi_i^j : X_i \to X_j$ for $1 \le i < j \le 5$ for different types of Π.

As expected, the quality of the approximation improves considerably as the number of integration points is increased. We also note that, for fixed coarse mesh $\mathcal{B}_i$, the error becomes smaller with increasing index j. This is obvious but cannot be seen in the figure as we do not intend to label all the single lines. Other than that, we do not experience any dependence on the mesh size. In particular, for the most critical combinations $(\mathcal{B}_i, \mathcal{B}_{i+1})_{1\le i\le 4}$, the errors depicted in Fig. 2 do not grow with increasing i.

The error decay is slightly different for the six transfer operators because both the coarse-to-fine integrand (e.g., $\lambda_p^j \lambda_q^i$ for $\mathcal{Q}$ versus $\psi_p^j \lambda_q^i$ for $\mathcal{P}$) and the form of the error transport vary (e.g., inverse mass matrix for $\mathcal{Q}$ versus diagonal scaling for $\widetilde{\mathcal{Q}}$). Regard-

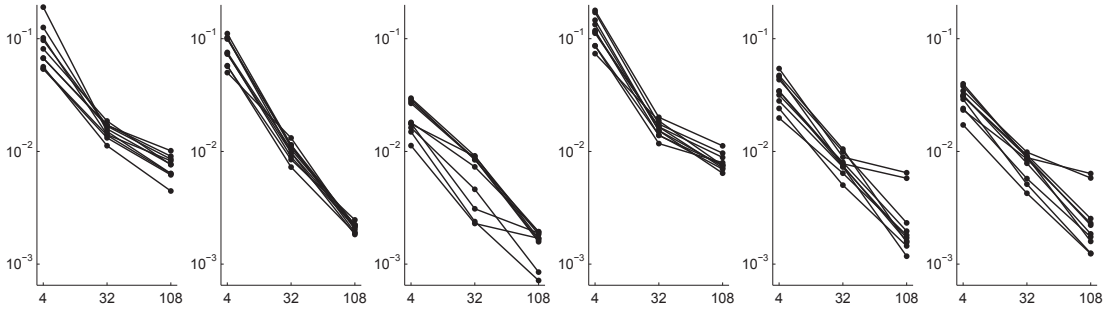

Figure 2: Estimated relative errors with respect to $|\cdot|_{H^1}$ of the operators $\mathcal{Q}$, $\mathcal{P}$, $\widetilde{\mathcal{Q}}$, $\mathcal{R}_{r=0}$, $\mathcal{R}_{r=1}$ and $\mathcal{R}_{r=2}$ (from left to right) depending on the number of integration points per element. Each line represents the error decay in one of the combinations $(\mathcal{B}_i, \mathcal{B}_j)_{1\leq i<j\leq 5}$.

less, we note that the composite quadrature rules produce very accurate approximations of the operators. The relative errors in the operators with respect to $|\cdot|_{H^1}$ are of the order of 1% or less; the errors with respect to $\|\cdot\|_{L^2}$ (not shown here) are even smaller.

3.4. Quantitative analysis of the relations between the transfer operators

In this section, we present a quantitative study of the diverse transfer operators. This eventually allows for arranging them in a map-like sketch illustrating similarities and differences. In the charts designed for this purpose, the operators are marked by the symbols and with the colors specified in Table 2 where they appear. Where applicable, the operators are evaluated using a composite quadrature formula with $m = 4$ as discussed in the previous section.

Table 2: Symbols and colors of the operators in the charts.

$\mathcal{I}$	$\mathcal{R}_{r=0}$	$\mathcal{R}_{r=1}$	$\mathcal{R}_{r=2}$	$\mathcal{Q}$	$\widetilde{\mathcal{Q}}$	$\mathcal{P}$
circle ∘	plus +	square □	crossing ×	diamond ◊	triangle △	dot •
(black)	**(orange)**	**(green)**	**(red)**	**(petrol)**	**(purple)**	**(blue)**
Section 2.1	Section 2.2	Section 2.2	Section 2.2	Section 2.3	Section 2.4	Section 2.5

Remark 3.1. To illustrate that the relations between the employed meshes are sufficiently general, we consider rotations of the mesh $\mathcal{B}_4$ about the axis spanned by the sum of the standard basis vectors $(\boldsymbol{e}_i)_{1\leq i\leq 3}$ by different, arbitrarily chosen angles. Table 3 states several relative differences for operators between these rotated meshes (for the angles specified at the head) and the meshes $\mathcal{B}_5$ and $\mathcal{B}_6$. If there were distinguished relations between the unrotated mesh and (some of) the other meshes, one would expect the computed quantities to vary more significantly. This is not the case in this study and the other studies we performed.

Table 3: The setting is sufficiently general. The computed estimates of the operator norms are independent of rotations of the meshes. We show exemplarily the relative differences between $\mathcal{P}$ and $\mathcal{Q}$ and between $\widetilde{\mathcal{Q}}$ and $\mathcal{Q}$ w.r.t. $|\cdot|_{H^1}$ (top) and $\|\cdot\|_{L^2}$ (bottom), respectively, between meshes of different sizes.

	0°	1°	2°	3°	4°	9.7°	17.1°	41.3°
$\lvert\mathcal{P}_4^5 - \mathcal{Q}_4^5\rvert_{H^1}/\lvert\mathcal{Q}_4^5\rvert_{H^1}$	0.29	0.29	0.30	0.30	0.30	0.26	0.31	0.32
$\lvert\widetilde{\mathcal{Q}}_4^5 - \mathcal{Q}_4^5\rvert_{H^1}/\lvert\mathcal{Q}_4^5\rvert_{H^1}$	0.61	0.61	0.61	0.63	0.64	0.62	0.59	0.61
$\lvert\mathcal{P}_4^6 - \mathcal{Q}_4^6\rvert_{H^1}/\lvert\mathcal{Q}_4^6\rvert_{H^1}$	0.29	0.29	0.28	0.27	0.26	0.25	0.28	0.28
$\lvert\widetilde{\mathcal{Q}}_4^6 - \mathcal{Q}_4^6\rvert_{H^1}/\lvert\mathcal{Q}_4^6\rvert_{H^1}$	0.58	0.58	0.57	0.58	0.58	0.57	0.60	0.58
$\lVert\mathcal{P}_4^5 - \mathcal{Q}_4^5\rVert_{L^2}/\lVert\mathcal{Q}_4^5\rVert_{L^2}$	0.25	0.26	0.25	0.25	0.24	0.24	0.24	0.24
$\lVert\widetilde{\mathcal{Q}}_4^5 - \mathcal{Q}_4^5\rVert_{L^2}/\lVert\mathcal{Q}_4^5\rVert_{L^2}$	0.53	0.53	0.53	0.54	0.55	0.55	0.53	0.53
$\lVert\mathcal{P}_4^6 - \mathcal{Q}_4^6\rVert_{L^2}/\lVert\mathcal{Q}_4^6\rVert_{L^2}$	0.21	0.21	0.21	0.21	0.21	0.21	0.21	0.20
$\lVert\widetilde{\mathcal{Q}}_4^6 - \mathcal{Q}_4^6\rVert_{L^2}/\lVert\mathcal{Q}_4^6\rVert_{L^2}$	0.50	0.50	0.50	0.50	0.50	0.50	0.49	0.50

Now, for each geometric shape and then each of the following choices of two finite element meshes, $(\mathcal{B}_i, \mathcal{B}_j)$, $(\mathcal{C}_i, \mathcal{C}_j)$ and $(\mathcal{H}_i, \mathcal{H}_j)$, $1 \leq i < j \leq 9$, we consider the distances of the generated operators $\mathcal{I}_i^j$, $(\mathcal{R}_{r=0})_i^j$, $(\mathcal{R}_{r=1})_i^j$, $(\mathcal{R}_{r=2})_i^j$, $\widetilde{\mathcal{Q}}_i^j$, and $\mathcal{P}_i^j$ to the L^2-projection $\mathcal{Q}_i^j$ between the spaces X_i and X_j. Fig. 3 and Fig. 4 show the relative differences with respect to $|\cdot|_{H^1}$ and $\|\cdot\|_{L^2}$, respectively. The diagrams are arranged such that a section marked by either $\mathcal{B}_i$ or $\mathcal{C}_i$ or $\mathcal{H}_i$ below (for some index i) comprises the results for all the situations $(\mathcal{B}_i, \mathcal{B}_j)_{i<j}$ or $(\mathcal{C}_i, \mathcal{C}_j)_{i<j}$ or $(\mathcal{H}_i, \mathcal{H}_j)_{i<j}$, each time ordered by increasing j from left to right.

We point out two distinct facts established by the performed experiments and readily understood by the figures. First, with decreasing ratio between fine and coarse mesh size, all depicted operators approximate $\mathcal{Q}$ more accurately. This is because they have the common property to preserve the constant functions, which has been mentioned before. In a certain sense, a very fine mesh is "almost nested" in a very coarse mesh and the coarse function is "almost constant" in the patches of the fine mesh; thus, the operators asymptotically become more and more like the identity if the coarse mesh is fixed.

The second, even more important result is the following. We see that, consistently for all experiments, the pseudo-L^2-projection is clearly the closest to the actual L^2-projection. In fact, it is remarkable how much closer this operator is to the orthogonal projection compared to all other approaches. The standard interpolation and the Clément-type interpolation with local polynomial degree $r = 2$, although being only moderately close to each other as we show shortly, have a very similar distance to $\mathcal{Q}$. These two operators are the next closest to the orthogonal projection; they are roughly twice as far away from $\mathcal{Q}$ as the pseudo-L^2-projection is. The others are considerably further away.

Another important point is that the ratio between fine and coarse mesh size is most relevant for the considered distances but not the mesh size itself. This is illustrated in Fig. 5 and Fig. 6. Here, we have collected several cases, each of four mesh combinations, each with a roughly comparable ratio of the numbers of elements. The ranges

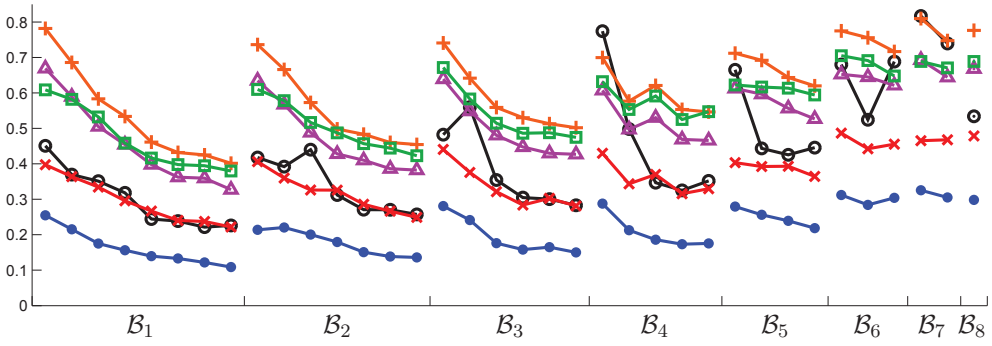

(a) Ball

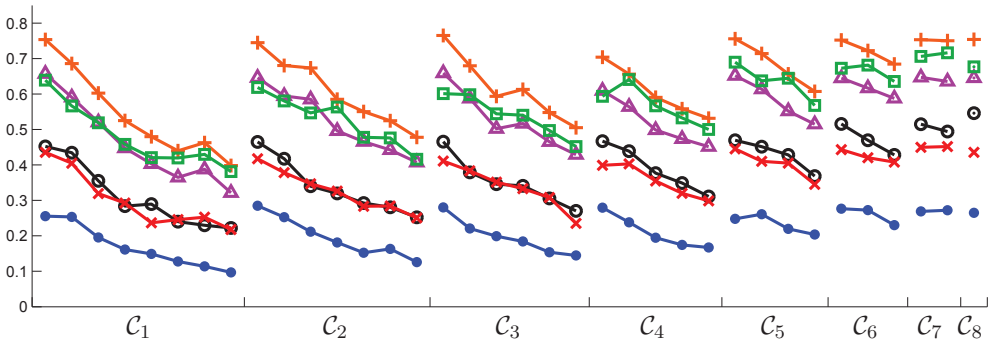

(b) Cylinder

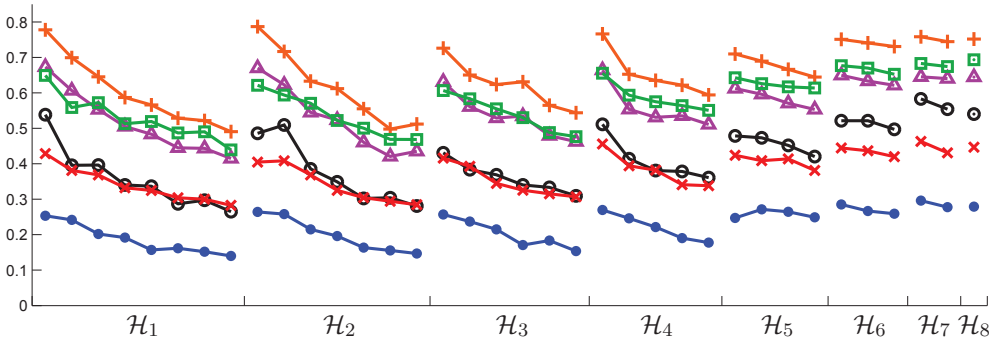

(c) Half torus

Figure 3: Relative distances to the L^2-projection $\mathcal{Q}$ with respect to $|\cdot|_{H^1}$ for the meshes from Table 1. Each marker represents one measurement (for example, the first blue dot marks $|\mathcal{P}_1^2 - \mathcal{Q}_1^2|_{H^1}/|\mathcal{Q}_1^2|_{H^1}$, the tenth black circle is $|\mathcal{I}_2^4 - \mathcal{Q}_2^4|_{H^1}/|\mathcal{Q}_2^4|_{H^1}$ and so forth). The labels $(\mathcal{B}_i)_{1\leq i\leq 9}$, $(\mathcal{C}_i)_{1\leq i\leq 9}$ and $(\mathcal{H}_i)_{1\leq i\leq 9}$ indicate the sections where the particular space X_i is the same. In each of these sections, the results are given for increasing j from left to right.

of this ratio are given in the description of Fig. 5. The classification is somewhat arbitrary; however, the diagrams show that the approximate differences to $\mathcal{Q}$ and $\mathcal{R}_{r=2}$, respectively, do not vary significantly in the considered situations. Note that all charts have the same scale on the vertical axes. As one has seen before in Fig. 3, the behavior of $\mathcal{I}$ appears to be the least predictable.

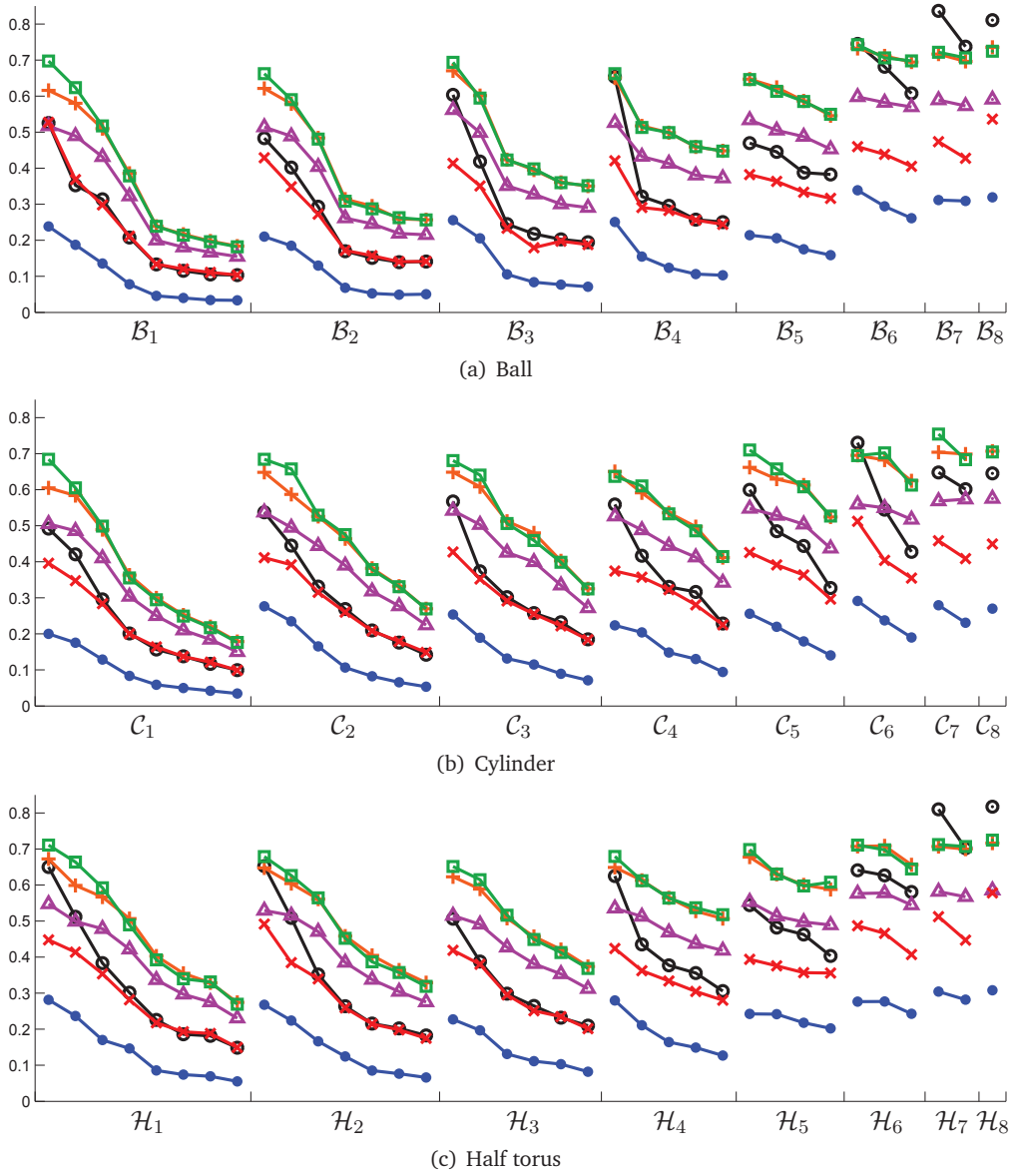

(a) Ball

(b) Cylinder

(c) Half torus

Figure 4: Relative distances to the L^2-projection $\mathcal{Q}$ with respect to $\|\cdot\|_{L^2}$ (cf. Fig. 3).

Finally, to highlight the interconnections, we state the complete data, namely the mutual relative distances between the operators with respect to $|\cdot|_{H^1}$, for one typical setting. The results for the mappings generated between the spaces associated with $\mathcal{B}_3$ and $\mathcal{B}_7$ are given in Table 4 ordered by their proximity to the L^2-orthogonal projection. In each cell, we state the relative difference of the two specified operators with respect to the one in the current row. Please be assured that this example is indeed representative.

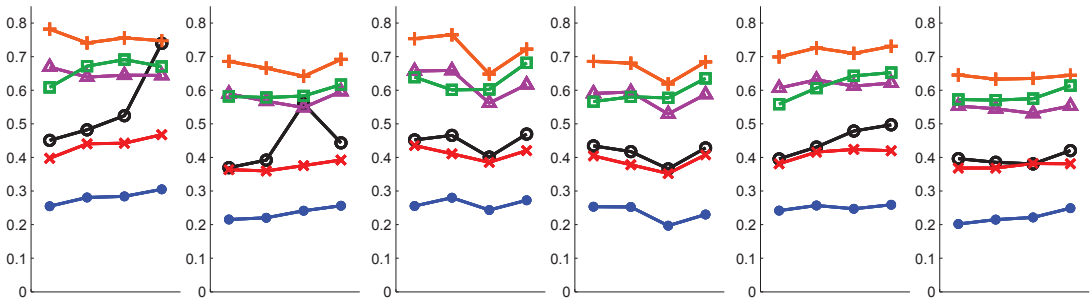

(a) Ball (b) Cylinder (c) Half torus

Figure 5: Relative distances to $\mathcal{Q}$ with respect to $|\cdot|_{H^1}$ in selected situations. For the four cases within each diagram, the ratio of the numbers of elements is roughly comparable. The ranges of this ratio are the following: Ball: 1.9 to 2.1 (left); 5.8 to 6.3 (right). Cylinder: 3.0 to 3.4 (left); 5.9 to 6.3 (right). Half torus: 2.7 to 3.3 (left); 8.7 to 9.9 (right).

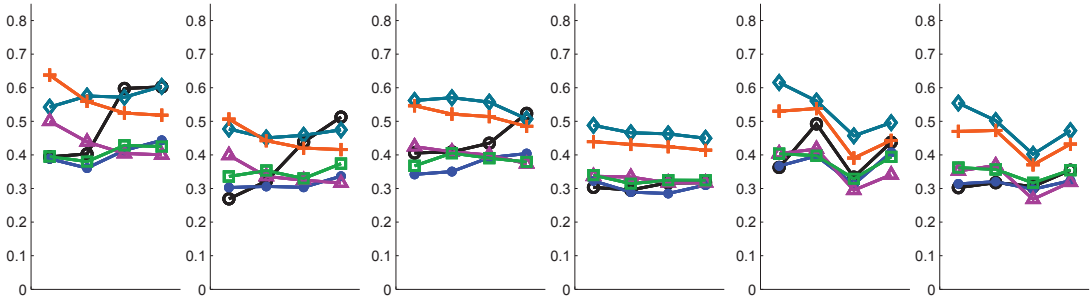

(a) Ball (b) Cylinder (c) Half torus

Figure 6: Relative distances to $\mathcal{R}_{r=2}$ with respect to $|\cdot|_{H^1}$ in selected situations (cf. Fig. 5).

Table 4: Relative distances w.r.t. $|\cdot|_{H^1}$ of the operators to each other in the situation $(\mathcal{B}_3, \mathcal{B}_7)$. The operators are ordered by their proximity to $\mathcal{Q}$. The value in a cell is relative to the operator specified by the row.

	$\mathcal{Q}$	$\mathcal{P}$	$\mathcal{R}_{r=2}$	$\mathcal{I}$	$\widetilde{\mathcal{Q}}$	$\mathcal{R}_{r=1}$	$\mathcal{R}_{r=0}$
$\mathcal{Q}$		0.16	0.28	0.30	0.45	0.49	0.53
$\mathcal{P}$	0.17		0.22	0.21	0.39	0.47	0.49
$\mathcal{R}_{r=2}$	0.32	0.23		0.22	0.23	0.26	0.31
$\mathcal{I}$	0.35	0.22	0.22		0.35	0.39	0.44
$\widetilde{\mathcal{Q}}$	0.52	0.41	0.23	0.36		0.24	0.10
$\mathcal{R}_{r=1}$	0.55	0.48	0.26	0.39	0.24		0.29
$\mathcal{R}_{r=0}$	0.61	0.51	0.32	0.45	0.10	0.30	

This section is concluded with a sketch summarizing the overall state. We visualize the interconnections between the transfer operators by Fig. 7. In this map-like graph, the lengths of the lines represent the distances of the connected operators with respect to $|\cdot|_{H^1}$. We pick a typical situation; here, the operators generated from $\mathcal{B}_3$ to $\mathcal{B}_7$

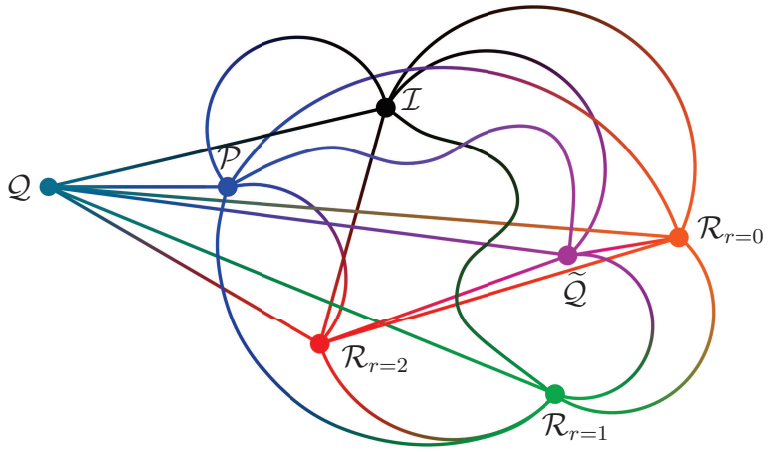

Figure 7: The mutual relations of the single operators visualized as a map-like graph. The length of each connecting line represents the H^1-distance between the respective operators. The lines from or to the L^2-orthogonal projection $\mathcal{Q}$ are straight.

are considered. The studies throughout the paper confirm that other situations or some averages yield essentially the same result as the sizes of the mutual distances are reasonably stable.

4. Numerical studies for a complex geometry: the Stanford Bunny

In this section, we present numerical studies for the widely used bunny model provided by the Stanford 3D Scanning Repository [55]. This is done to further demonstrate that the results seem to be largely independent of the underlying computational domain.

The original geometry data from [55] describes a surface with boundary by 69,451 triangles. (There are five holes in the lower part of the geometry.) We want to consider "the interior" of this surface as 3D computational domain. For this purpose, we fixed the holes to obtain a closed surface which is the boundary of a simply connected domain with the shape of the Stanford Bunny. This surface is in an intermediate step approximated sufficiently accurately using NURBS, which is fairly standard in industrial applications.

Then, as done in Section 3.1 for the simpler geometric shapes, unstructured volume meshes are generated by standard tools from CUBIT [51]. We use the seven tetrahedral meshes $(\mathcal{S}_i)_{1\leq i\leq 7}$ with their characteristics given in Table 5 ordered by the number of elements. They are again completely independent of each other and cover a broad range of sizes. Two of the meshes are illustrated in Fig. 8.

Proceeding as in Section 3, we study the mutual relations between the different transfer operators when evaluated between the finite element spaces associated with pairs of meshes $(\mathcal{S}_i, \mathcal{S}_j)_{1\leq i<j\leq 7}$. Fig. 9 shows the relative distances of the operators to

Table 5: Stanford Bunny: Characteristics of the independently generated meshes $(\mathcal{S}_i)_{1\leq i\leq 7}$.

	#elements	#nodes
$\mathcal{S}_1$	6,447	1,479
$\mathcal{S}_2$	12,732	2,720
$\mathcal{S}_3$	26,355	5,380
$\mathcal{S}_4$	41,256	8,216
$\mathcal{S}_5$	83,213	16,095
$\mathcal{S}_6$	124,576	23,856
$\mathcal{S}_7$	184,783	34,860

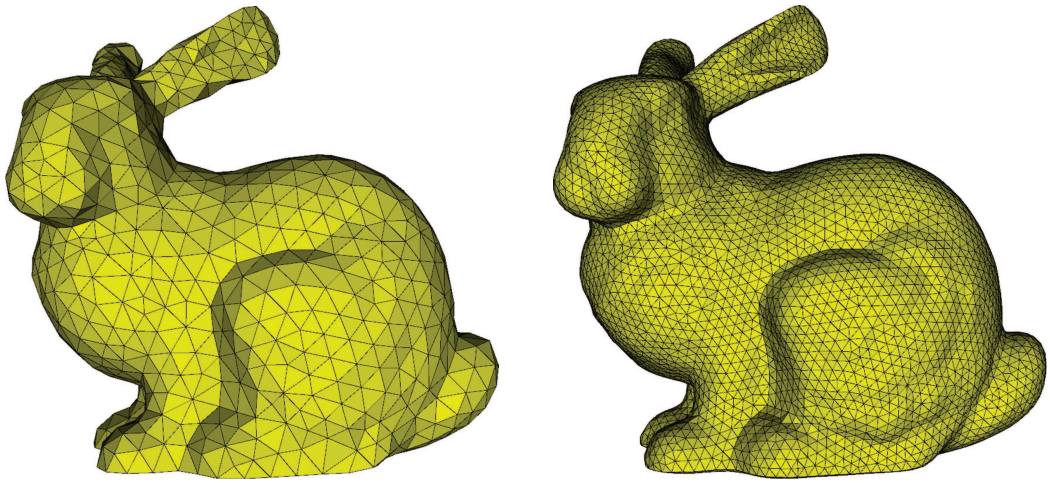

Figure 8: Stanford Bunny [55]: Examples for the meshes of Table 5. We show $\mathcal{S}_2$ (left) and $\mathcal{S}_6$ (right).

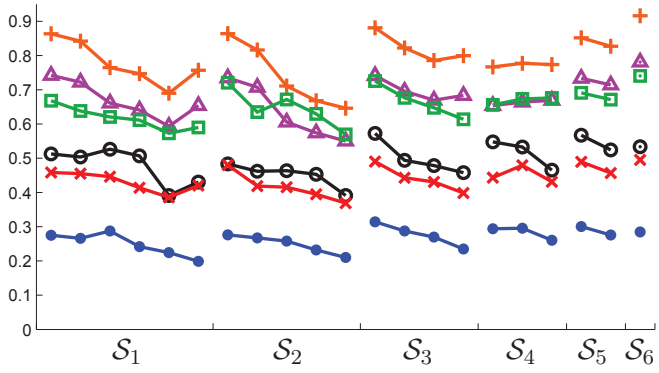

Figure 9: Stanford Bunny: Relative distances to the L^2-projection $\mathcal{Q}$ with respect to $|\cdot|_{H^1}$ (cf. Fig. 3).

the L^2-projection with respect to $|\cdot|_{H^1}$. The results are very similar to the ones obtained earlier for the simpler geometric shapes; cf. Fig. 3. The other findings of Section 3.4 hold true for the study of the Stanford Bunny, too. In particular the other measured distances are very similar (not shown here).

5. Conclusion

To investigate the information transfer between finite element spaces associated with non-nested meshes, we examined a variety of transfer operators. The numerical studies provided insight into their mutual relations. We considered the standard (nodal) finite element interpolation, Clément's quasi-interpolation with different local polynomial degrees, the global L^2-orthogonal projection, a local L^2-quasi-projection via a discrete inner product motivated by a quadrature rule, and a pseudo-L^2-projection defined by a Petrov-Galerkin variational equation with a discontinuous test space. We reviewed basic properties of the operators and pointed out conceptual and implementational similarities and differences. The comprehensive computational comparison of the transfer operators showed that the differences between them are substantial. For the presented geometric test cases in 3D (unstructured meshes of ball, cylinder, half torus and Stanford Bunny), the pseudo-L^2-projection turned out to be clearly the closest to the actual L^2-projection compared to all other operators.

Acknowledgments This work was partly supported by the Bonn International Graduate School in Mathematics and by the Iniziativa Ticino in Rete. We would like to thank the participants of the Söllerhaus Workshop on Domain Decomposition Methods in October 2011 and an anonymous referee for useful remarks on the topic of this paper. We appreciate the help of Johannes Steiner in preparing the Stanford Bunny for the experiments.

References

[1] Adams, R.A.: Sobolev Spaces. Academic Press, New York (1975)
[2] Ainsworth, H.: Octree C++ General Component (2005)
[3] Apel, T.: Anisotropic Finite Elements: Local Estimates and Applications. Advances in Numerical Mathematics. Teubner, Stuttgart (1999)
[4] Apel, T.: Interpolation in h-version finite element spaces. In: E. Stein, R. de Borst, T.J.R. Hughes (eds.) Encyclopedia of Computational Mechanics. Vol. 1. Fundamentals, pp. 55–72. Wiley, Chichester (2004)
[5] Bank, R.E., Dupont, T.F., Yserentant, H.: The hierarchical basis multigrid method. Numer. Math. **52**(4), 427–458 (1988)
[6] Barber, C.M., Dobkin, D.P., Huhdanpaa, H.: The quickhull algorithm for convex hulls. ACM Trans. Math. Softw. **22**(4), 469–483 (1996)
[7] Bastian, P., Birken, K., Johannsen, K., Lang, S., Neuß, N., Rentz-Reichert, H., Wieners, C.: UG – a flexible software toolbox for solving partial differential equations. Comput. Vis. Sci. **1**(1), 27–40 (1997)
[8] Ben Belgacem, F.: The mortar finite element method with Lagrange multipliers. Numer. Math. **84**(2), 173–197 (1999)
[9] Bernardi, C., Maday, Y., Patera, A.T.: A new nonconforming approach to domain decomposition: the mortar element method. In: H. Brezis, J.L. Lions (eds.) Nonlinear Partial Differential Equations and Their Applications, *Pitman Res. Notes Math. Ser.*, vol. 299, pp. 13–51. Harlow: Longman Scientific & Technical, New York (1994)

[10] Braess, D.: Finite Elemente. Springer, Berlin (2007)
[11] Braess, D., Verfürth, R.: Multigrid methods for nonconforming finite element methods. SIAM J. Numer. Anal. **27**(4), 979–986 (1990)
[12] Bramble, J.H., Pasciak, J.E., Steinbach, O.: On the stability of the L^2-projection in $H^1(\Omega)$. Math. Comp. **71**(237), 147–156 (2002)
[13] Bramble, J.H., Pasciak, J.E., Vassilevski, P.S.: Computational scales of Sobolev norms with applications to preconditioning. Math. Comp. **69**(230), 463–480 (2000)
[14] Bramble, J.H., Pasciak, J.E., Wang, J., Xu, J.: Convergence estimates for multigrid algorithms without regularity assumptions. Math. Comp. **57**(195), 23–45 (1991)
[15] Bramble, J.H., Pasciak, J.E., Xu, J.: The analysis of multigrid algorithms with nonnested spaces or noninherited quadratic forms. Math. Comp. **56**(193), 1–34 (1991)
[16] Bramble, J.H., Xu, J.: Some estimates for a weighted L^2 projection. Math. Comp. **56**(194), 463–476 (1991)
[17] Brandt, A.: Multi-level adaptive solutions to boundary-value problems. Math. Comp. **31**(138), 333–390 (1977)
[18] Brenner, S.C.: Convergence of nonconforming V-cycle and F-cycle multigrid algorithms for second order elliptic boundary value problems. Math. Comp. **73**(247), 1041–1066 (2004)
[19] Brenner, S.C., Scott, L.R.: The Mathematical Theory of Finite Element Methods, *Texts in Applied Mathematics*, vol. 15. Springer, Berlin (2002)
[20] X.-C. Cai: The use of pointwise interpolation in domain decomposition methods with non-nested meshes. SIAM J. Sci. Comput. **16**(1), 250–256 (1995)
[21] Carstensen, C.: Quasi-interpolation and a posteriori error analysis in finite element methods. Math. Model. Numer. Anal. **33**(6), 1187–1202 (1999)
[22] Carstensen, C.: Merging the Bramble-Pasciak-Steinbach and the Crouzeix-Thomée criterion for H^1-stability of the L^2-projection onto finite element spaces. Math. Comp. **71**(237), 157–163 (2002)
[23] Carstensen, C.: Clément interpolation and its role in adaptive finite element error control. In: E. Koelink, J. van Neerven, B. de Pagter, G. Sweers (eds.) Partial Differential Equations and Functional Analysis – The Philippe Clément Festschrift, *Oper. Theory Adv. Appl.*, vol. 168, pp. 27–43. Birkhäuser, Basel (2006)
[24] Chan, T.F., Smith, B.F., Zou, J.: Overlapping Schwarz methods on unstructured meshes using non-matching coarse grids. Numer. Math. **73**(2), 149–167 (1996)
[25] Ciarlet, P.G.: The Finite Element Method for Elliptic Problems, *Studies in Mathematics and its Applications*, vol. 4. North-Holland, Amsterdam (1978)
[26] Clément, P.: Approximation by finite element functions using local regularization. RAIRO Anal. Numér. **9**(R-2), 77–84 (1975)
[27] Cohen, A., Daubechies, I., Feauveau, J.C.: Biorthogonal bases of compactly supported wavelets. Comm. Pure Appl. Math. **45**(5), 485–560 (1992)
[28] Crouzeix, M., Thomée, V.: The stability in L^p and W_p^1 of the L^2-projection onto finite element function spaces. Math. Comp. **48**(178), 521–532 (1987)
[29] Dahmen, W., Kunoth, A., Urban, K.: Biorthogonal spline wavelets on the interval – stability and moment conditions. Appl. Comput. Harmon. Anal. **6**(2), 132–196 (1999)
[30] Dickopf, T.: Multilevel methods based on non-nested meshes. Ph.D. thesis, University of Bonn (2010). http://hss.ulb.uni-bonn.de/2010/2365
[31] Dickopf, T.: Nodal interpolation between first-order finite element spaces in 1d is uniformly H^1-stable. In: A. Cangiani, R.L. Davidchack, E. Georgoulis, A. Gorban, J. Levesley, M. Tretyakov (eds.) Numerical Mathematics and Advanced Applications, Proceedings of

ENUMATH 2011, pp. 419–427. Springer, Berlin (2012)
[32] Dickopf, T., Krause, R.: Efficient simulation of multi-body contact problems on complex geometries: a flexible decomposition approach using constrained minimization. Int. J. Numer. Methods Engrg. **77**(13), 1834–1862 (2009)
[33] Dickopf, T., Krause, R.: Weak information transfer between non-matching warped interfaces. In: M. Bercovier, M.J. Gander, R. Kornhuber, O.B. Widlund (eds.) Domain Decomposition Methods in Science and Engineering XVIII, *Lect. Notes Comput. Sci. Eng.*, vol. 70, pp. 283–290. Springer, Berlin (2009)
[34] Douglas jun., J., Dupont, T.F., Wahlbin, L.: The stability in L^q of the L^2-projection into finite element function spaces. Numer. Math. **23**(3), 193–197 (1975)
[35] Evans, L.C.: Partial Differential Equations, *Graduate Studies in Mathematics*, vol. 19. AMS, Providence, RI, USA (1998)
[36] Falletta, S.: The approximate integration in the mortar method constraint. In: O.B. Widlund, D.E. Keyes (eds.) Domain Decomposition Methods in Science and Engineering XVI, *Lect. Notes Comput. Sci. Eng.*, vol. 55, pp. 555–563. Springer, Berlin (2007)
[37] Flemisch, B., Wohlmuth, B.: Stable Lagrange multipliers for quadrilateral meshes of curved interfaces in 3D. Comput. Methods Appl. Mech. Eng. **196**(8), 1589–1602 (2007)
[38] Gander, M.J., Japhet, C.: An algorithm for non-matching grid projections with linear complexity. In: M. Bercovier, M.J. Gander, R. Kornhuber, O.B. Widlund (eds.) Domain Decomposition Methods in Science and Engineering XVIII, *Lect. Notes Comput. Sci. Eng.*, vol. 70, pp. 185–192. Springer, Berlin (2009)
[39] Griebel, M.: Multilevelmethoden als Iterationsverfahren über Erzeugendensystemen. Teubner Skripten zur Numerik. Teubner, Stuttgart (1994)
[40] Hackbusch, W.: Multi-Grid Methods and Applications, *Springer Series in Computational Mathematics*, vol. 4. Springer, Berlin (1985)
[41] Kim, C., Lazarov, R.D., Pasciak, J.E., Vassilevski, P.S.: Multiplier spaces for the mortar finite element method in three dimensions. SIAM J. Numer. Anal. **39**(2), 519–538 (2001)
[42] Knyazev, A.V.: Toward the optimal preconditioned eigensolver: Locally optimal block preconditioned conjugate gradient method. SIAM J. Sci. Comput. **23**(2), 517–541 (2001)
[43] Lamichhane, B.P.: Higher order mortar finite elements with dual lagrange multiplier spaces and applications. Ph.D. thesis, University of Stuttgart (2006)
[44] Lamichhane, B.P., Wohlmuth, B.: Biorthogonal bases with local support and approximation properties. Math. Comp. **76**(257), 233–249 (2007)
[45] Maday, Y., Rapetti, F., Wohlmuth, B.: The influence of quadrature formulas in 2d and 3d mortar element methods. In: L.F. Pavarino, A. Toselli (eds.) Recent Developments in Domain Decomposition Methods, *Lect. Notes Comput. Sci. Eng.*, vol. 23, pp. 203–221. Springer, Berlin (2002)
[46] Oswald, P.: Multilevel Finite Element Approximation. Theory and Applications. Teubner Skripten zur Numerik. Teubner, Stuttgart (1994)
[47] Oswald, P.: Intergrid transfer operators and multilevel preconditioners for nonconforming discretizations. Appl. Numer. Math. **23**(1), 139–158 (1997)
[48] Oswald, P.: Optimality of multilevel preconditioning for nonconforming P1 finite elements. Numer. Math. **111**(2), 267–291 (2008)
[49] Oswald, P., Wohlmuth, B.: On polynomial reproduction of dual FE bases. In: N. Debit, M. Garbey, R. Hoppe, J. Périaux, D.E. Keyes, Y. Kuznetsov (eds.) Thirteenth International Conference on Domain Decomposition Methods, pp. 85–96. CIMNE, Barcelona (2002)
[50] Ruge, J.W., Stüben, K.: Algebraic multigrid. In: S.F. McCormick (ed.) Multigrid Methods, *Frontiers in Applied Mathematics*, vol. 3, pp. 73–130. SIAM, Philadelphia, PA, USA (1987)

[51] Sandia National Laboratories: CUBIT (2012). http://cubit.sandia.gov
[52] Schenk, O., Gärtner, K.: Solving unsymmetric sparse systems of linear equations with PARDISO. Future Generation Computer Systems **20**(3), 475–487 (2004)
[53] Schenk, O., Gärtner, K.: On fast factorization pivoting methods for sparse symmetric indefinite systems. Electron. Trans. Numer. Anal. **23**, 158–179 (2006)
[54] Scott, L.R., Zhang, S.: Finite element interpolation of nonsmooth functions satisfying boundary conditions. Math. Comp. **54**(190), 483–493 (1990)
[55] Stanford 3D Scanning Repository: Stanford Bunny (1994). http://graphics.stanford.edu/data/3Dscanrep
[56] Steinbach, O.: On a generalized L^2-projection and some related stability estimates in Sobolev spaces. Numer. Math. **90**(4), 775–786 (2002)
[57] Steinbach, O.: Stability Estimates for Hybrid Coupled Domain Decomposition Methods, *Lecture Notes in Mathematics*, vol. 1809. Springer, Berlin (2003)
[58] Toselli, A., Widlund, O.B.: Domain Decomposition Methods – Algorithms and Theory, *Springer Ser. Comput. Math.*, vol. 34. Springer, Berlin (2005)
[59] Trottenberg, U., Oosterlee, C.W., Schüller, A.: Multigrid. Academic Press, Orlando (2001)
[60] Verfürth, R.: Error estimates for some quasi-interpolation operators. Math. Model. Numer. Anal. **33**(4), 695–713 (1999)
[61] Vujičić, M.: Linear Algebra Thoroughly Explained. Springer, Berlin (2008)
[62] Wohlmuth, B.: A mortar finite element method using dual spaces for the lagrange multiplier. SIAM J. Numer. Anal. **38**(3), 989–1012 (2000)
[63] Wohlmuth, B.: Discretization Methods and Iterative Solvers Based on Domain Decomposition, *Lect. Notes Comput. Sci. Eng.*, vol. 17. Springer, Berlin (2001)
[64] Xu, J.: Theory of multilevel methods. Ph.D. thesis, Cornell University (1989)
[65] Xu, J.: The auxiliary space method and optimal multigrid preconditioning techniques for unstructured grids. Computing **56**(3), 215–235 (1996)
[66] Yserentant, H.: Old and new convergence proofs for multigrid methods. Acta Numerica **2**, 285–326 (1993)